Vaccine-specific immune responses against *Mycobacterium ulcerans* infection in a low-dose murine challenge model.

Kirstie M. Mangas[1], Andrew H. Buultjens[1], Jessica L. Porter[1], Sarah L. Baines[1], Estelle Marion[2], Laurent Marsollier[2], Nicholas J. Tobias[3,4], Sacha J. Pidot[1], Kylie M. Quinn[5], David J. Price[6,7], Katherine Kedzierska[1], Weiguang Zeng[1], David C. Jackson[1], Brendon Y. Chua[1,*] and Timothy P. Stinear[1,*].

1. Department of Microbiology and Immunology, Doherty Institute, University of Melbourne
2. CRCINA, INSERM, Université de Nantes, Université d'Angers, Angers, France
3. Molekulare Biotechnologie, Fachbereich Biowissenschaften, Goethe-Universität Frankfurt, Frankfurt am Main, Germany
4. LOEWE Centre for Translational Biodiversity in Genomics (TBG), Germany
5. Monash Biomedicine Discovery Institute and Department of Biochemistry and Molecular Biology, Monash University, Clayton, VIC 3800, Australia.
6. Victorian Infectious Diseases Reference Laboratory Epidemiology Unit at The Peter Doherty Institute for Infection & Immunity, The University of Melbourne and Royal Melbourne Hospital, VIC 3000, Australia
7. Centre for Epidemiology & Biostatistics, Melbourne School of Population & Global Health, The University of Melbourne, VIC 3010, Australia

* Joint senior authors

Running title: Immune responses against Buruli ulcer

Abstract:

The neglected tropical disease Buruli ulcer (BU) is an infection of subcutaneous tissue with *Mycobacterium ulcerans*. There is no effective BU vaccine. Here, we assessed an experimental prime-boost vaccine in a low-dose murine tail infection model. We used the enoyl-reductase (ER) domain of the *M. ulcerans* mycolactone polyketide synthases electrostatically coupled with a previously described TLR-2 agonist-based lipopeptide adjuvant, R_4Pam2Cys. Mice were vaccinated and then challenged via tail inoculation with 14-20 colony forming units (CFU) of an engineered bioluminescent strain of *M. ulcerans*. Mice receiving either the experimental ER vaccine or *Mycobacterium bovis* Bacille Calmette-Guérin (BCG) were equally well protected, with both groups faring significantly better than non-vaccinated animals ($p<0.05$). A suite of 29 immune parameters were assessed in the mice at the end of the experimental period. Multivariate statistical approaches were then used to interrogate the immune response data to develop disease-prognostic models. High levels of IL-2 and low IFN-**γ** produced in the spleen best predicted control of infection across all vaccine groups. Univariate logistic regression then revealed vaccine-specific profiles of protection. High titres of ER-specific IgG serum antibodies together with IL-2 and IL-4 in the draining lymph node (DLN) were associated with protection induced by the experimental ER vaccine. In contrast, high titres of IL-6, TNF-**α**, IFN-**γ** and IL-10 in the DLN and low IFN**γ** titres in the spleen were associated with protection following BCG vaccination. This study suggests an effective BU vaccine must induce localized, tissue-specific immune profiles with controlled inflammatory responses at the site of infection.

Introduction:

Buruli ulcer (BU) is a disease primarily of the subcutaneous tissue caused by infection with *Mycobacterium ulcerans*. BU initially presents as redness of the skin that is often accompanied with oedema and swelling. As the disease progresses, oedema may increase or an open ulcer develop (1, 2), the latter is typically characterised by deep undermined edges with a necrotic core comprised of bacteria, dead skin cells and immune cells (3, 4). Ulcers are predominately found on the extremities of the body such as the upper (27% of cases) and lower limbs (70% of cases) (5). The disease is rarely fatal, but if left untreated extensive destruction of subcutaneous tissue can leave victims with significant deformities and lifelong disabilities (3, 6-9).

BU is likely caused when *M. ulcerans* is introduced beneath the skin. This can occur if a region of contaminated skin surface is punctured or by insertion of an object contaminated with the bacteria into subcutaneous tissue (*e.g.* via an insect bite) (10-12). BU-endemic areas include certain regions of West and Sub-Saharan Africa and south eastern Australia (13, 14).

M. ulcerans is a slow-growing bacterium, with a doubling time greater than 48 hours (15, 16) making it difficult for early disease diagnosis as symptoms can take between 4-5 months to appear after primary infection (17, 18). If diagnosed early, however, BU can be treated effectively by combination antibiotic therapy (19-21). Unfortunately, in many cases the disease can initially be misdiagnosed as other, more common skin infections. Additionally, a large proportion of BU cases in African countries occur in rural villages and poorer areas with limited or no access to health care, with patients facing disfigurement and permanent disability. Given that diagnoses are delayed and usually occur after a lesion has become relatively advanced and ulceration extensive (22), development of an effective BU vaccine to protect those in highly endemic areas is of paramount importance.

Currently, the only licensed vaccine against mycobacterial infections approved for human use is the *M. bovis*-derived Bacille Calmette-Guérin (BCG) vaccine for prevention of tuberculosis. This vaccine is cross-protective against *M. ulcerans*, but only delays the onset of disease (23-25). Several experimental vaccines have been tested against *M. ulcerans* infection, as summarised in Table 1. Although different animal models have been utilised to study *M. ulcerans* infections including guinea pig, primate, pig and armadillo (10, 23, 26-31), most studies assessing vaccine efficacy have used mice. Vaccines tested in these murine challenge models have included DNA-based, viral-based, protein subunit and whole cell vaccines (25, 32-35) (Table 1). Among the various vaccines, BCG expressing *M. ulcerans* antigens appears to offer the best protective effect against challenge. Hart et al. (36, 37) showed enhanced protection against BU using a recombinant BCG vaccine that expressed *M. ulcerans* Ag85A or recombinant Ag85B-EsxH fusion protein in a mouse footpad challenge model. Whilst improving the immunogenicity of BCG may be a promising route, there are also some drawbacks; exposure to environmental mycobacteria is believed to decrease the efficacy of the BCG vaccine and administration in areas where people have been BCG-exposed may be problematic (38).

M. ulcerans causes disease primarily through the production of a lipid toxin called mycolactone (39). Mycolactone modulates cell function, in particular secretion of critical cytokines by specifically inhibiting the Sec61 translocon, enabling *M. ulcerans* to escape host immune defences (40-46). The toxin is formed from simple acetate and propionate precursors by three polyketide synthases (PKS) encoded by genes on the plasmid pMUM001 (47, 48). Within each PKS are enzymatic domains that form the mycolactone molecule. Some of these domains have been found to be immunogenic and in particular immune responses against the enoyl reductase (ER) domain have previously been shown to significantly reduce *M. ulcerans* bacterial load in the footpad of a murine prime-boost

98 vaccination study (49). Based on the immunogenic and protective qualities of ER, we have utilised
99 it as a target antigen for a BU subunit vaccine.
100
101 Protein antigens generally require an adjuvant to boost immunogenicity and shape immune
102 responses. A known TLR-2 ligand, R_4Pam_2Cys, has been previously shown to induce robust antibody
103 responses as well as augmented $CD4^+$ and $CD8^+$ T cell responses, possibly through promoting
104 dendritic cell antigen uptake and trafficking to lymph nodes (50, 51). Given BU is a disease where
105 the bacteria can be both extracellular and intracellular, the ability of R_4Pam_2Cys to robustly engage
106 multiple arms of the adaptive immune system may be beneficial for a BU subunit vaccine.
107
108 Previous research has shown that as few as three colony forming units (CFU) of bacteria are required
109 to initiate infection (10), however most animal models challenge with $>10^4$ CFU (see Table 1) (25,
110 32-37, 49, 52-54). This dose is likely to be far higher than the dose of bacteria that leads to natural
111 infection in humans and other animals (10). Such an unrealistic high dose may overwhelm immune
112 responses and underestimate the true efficacy of potential *M. ulcerans* vaccines. For these reasons,
113 we have used a low-dose of *M. ulcerans* in a tail infection challenge model to evaluate an
114 experimental prime-boost subunit vaccine against BU. The experimental subunit vaccine developed
115 here comprised of the *M. ulcerans* mycolactone ER domain protein formulated with the adjuvant,
116 R_4Pam_2Cys. Our murine challenge model with physiologically relevant dosing enabled us to more
117 accurately measure vaccine-induced protection and to explore immune correlates of protection
118 against BU.
119
120

Results:

Formulation of the ER-R_4Pam_2Cys subunit vaccine candidate

Mycolactone is the key virulence factor produced by *M. ulcerans* and an attractive vaccine target, but the molecule is poorly immunogenic (55). However, the PKS enzymes used by the bacterium to synthesize mycolactones – are highly conserved and immunogenic (49, 56-58). Therefore, we hypothesized that targeting the conserved enzymatic domains of the mycolactone PKS could be an effective vaccine strategy. One domain in particular, the enoyl reductase (ER) protein domain, elicits serum antibodies in BU patients and healthy controls in BU endemic regions (57). The ER protein expressed as an antigen in a DNA-protein prime-boost vaccine has also been shown to reduce bacterial burden in a mouse footpad *M. ulcerans* challenge model (49). Here, we utilised the ER protein to create a novel BU vaccine candidate by electrostatically associating it with the TLR-2 agonist-based lipopeptide R_4Pam_2Cys. To formulate this vaccine, recombinant 6xHis-tagged ER protein (37 kDa) was first produced and confirmed by SDS-PAGE (Fig. 1A) and western blotting (Fig. 1B). This protein antigen was formulated with R_4Pam_2Cys at various ratios to firstly optimise the formation of protein-lipopeptide complexes. A ratio of 1:1 was sufficient to produce complexes that were larger in size than each constituent on its own (Fig. 1C). While the majority of these complexes were ~300nm in radius (peak 5), the presence of smaller sized particles of ~100nm (peak 4) suggests that not all antigen was incorporated within a complex as this size range corresponds to the size of ER protein (peak 3) or R_4Pam_2Cys alone (peak 2). Although a 1:3 ratio appears to be more effective for the association of these constituents, the size distribution of form complexes was not monodispersed and appeared as two distinct populations (peak 6 and 7). A 1:5 ratio, however, produced a uniform population of complexes that were ~500 nm in radius (peak 8) and this formulation was subsequently used to vaccinate animals.

Evaluation of ER-specific antibody responses in vaccinated mice

To evaluate the ability of the vaccine to induce ER-specific antibody responses, mice were vaccinated, and sera obtained after priming and boosting with the subunit vaccine. Our results showed that primary vaccination with ER + R_4Pam_2Cys resulted in significantly higher levels of ER-specific antibody compared to vaccination with unadjuvanted ER antigen (p<0.0001) (Fig. 1D). In fact, there was no significant difference in responses between unvaccinated mice and those vaccinated with a single dose of ER alone, R_4Pam_2Cys only or BCG. Although a second dose of ER alone was able to increase these responses, the titres were still ~100-fold less than levels achieved by boosting mice with ER + R_4Pam_2Cys (p<0.0001). These results not only indicate that ER-specific antibodies can be generated in mice and that the use of R_4Pam_2Cys can significantly enhance these responses, but that BCG does not induce cross-reactive antibodies to the ER protein.

Characterisation of a low-dose M. ulcerans murine tail infection model

We have previously described the use of a low-dose tail infection model for studying insect-mediated transmission of *M. ulcerans* (10). We reasoned that because BU patients were likely to be initially infected with a low bacterial inoculum (10, 11, 59) we could use this model to test the protective efficacy of responses induced by the ER + R_4Pam_2Cys vaccine. This model features the use of a bioluminescent strain of *M. ulcerans* (10, 60) and its infectious characteristics are summarised in Fig. 2. Compared to an uninfected tail (Fig 2A and C), sub-cutaneous infection of a tail results in the appearance of a visible ulcer (Fig 2B) exhibiting the highest levels of bioluminescence concentrated around the centre of the lesion (Fig 2D), i.e. where swelling appears to be the greatest, and beginning to diminish around the periphery reflecting a positive correlation between bacterial burden and light emission (61). Histological cross-sections revealed that while tissue integrity of an uninfected tail appears defined and intact (Fig. 2E & F), dramatic differences are observed in the infected tail, typified by loss of muscle, vasculature and epidermis structure and disruptions to surrounding connective tissue (Fig. 2G & H). Further examination of this tissue

showed the presence of acid-fast bacilli as well as an infiltration of polymorphonuclear cells (PMNs) (Fig. 2I). Despite evidence of bacteria engulfment by these cells (Fig. 2J), it would appear that this response was insufficient for controlling the infection and preventing disease progression.

Monitoring vaccine efficacy using bioluminescent M. ulcerans and in vivo imaging system (IVIS)

We have previously established a correlation between *M. ulcerans* bioluminescence and bacterial burden (61). Here, we set a threshold of ≥ $5x10^5$ photons/second (equivalent to $2.8x10^5$ CFU) as a measure of ineffective disease control, *i.e.* appearance of disease. Mice were vaccinated subcutaneously and then challenged with an estimated 17 CFU (range 14-20 CFU) of bioluminescent *M. ulcerans* via intradermal tail inoculation. Animals were monitored weekly for changes in bioluminescence using IVIS for up to 24 weeks. Fig. 3A shows an example of the progression of bioluminescence (and therefore disease) in an unvaccinated mouse, up to week 16 whereupon the clinical endpoint of the experiment was reached. Bioluminescence for all mice was recorded across the experimental period. Plots for the different treatment groups show the progression in bioluminescence over time (Fig3B-F). Mice from the ER alone, R_4Pam_2Cys alone and unvaccinated treatment groups displayed the first detectable bioluminescence at week 7. There also appeared to be threshold in bioluminescence, whereby animals expressing ≥$5x10^5$ photons/second from tail lesions became less able to control the infection and progressed to the clinical endpoint (Fig. 3B). The immune response data for all mice is provided (Supplementary Table S1). Using these data, failure-to-protect was defined as tail bioluminescence equal to or greater than $5x10^5$ photons/second at or before week 24 (end of experiment). Therefore, mice were defined as 'protected' if bioluminescence was less than $5x10^5$ photons/second at week 24.

Vaccination with ER + R_4Pam_2Cys offers similar protection to M. bovis BCG vaccine

Survival analysis was conducted to assess vaccine efficacy by measuring the time from infection until tail bioluminescence at the threshold of $5x10^5$ photons/second was reached. Mice that reached this threshold were defined as 'not protected'. Significantly less ER + R_4Pam_2Cys vaccinated mice (4/10 animals) developed disease compared to unvaccinated mice (9/10 animals), indicating ER + R_4Pam_2Cys provided some level of protection against disease progression compared to no vaccination (Fig. 3B, E & G) ($p<0.01$). Mice vaccinated with BCG were best protected with only 1 animal exceeding the bioluminescence threshold (Fig. 3F & G). Although this number of mice was reduced compared to the ER + R_4Pam_2Cys vaccinated animals, the difference was not significant (Fig. 3G). However, the bacterial burden (as indicated by mean photon counts/sec at the clinical endpoint) in BCG vaccinated mice was lower than animals that received the ER + R_4Pam_2Cys vaccine (means: $6x10^5$ [n=2, range 3.5 – $8.6x10^5$] versus $3.3x10^7$ [n=3, range 2.4 - $4.1x10^7$] photons/sec respectively) suggesting the protective superiority of BCG. There was also no significant difference between the protective efficacy of vaccination with ER alone compared with ER + R_4Pam_2Cys, although mice vaccinated with the latter exhibited delayed disease progression (onset at weeks 16-24) compared to ER vaccinated mice (onset at weeks 8- 16) indicating that formulation of the antigen with the R_4Pam_2Cys adjuvant improved immunity (Fig. 3D, E).

Measuring immune parameters following vaccination and challenge

At the experimental end-point, sera, spleens and draining lymph nodes (DLN) from all animals were collected and several parameters were further analysed; ER-specific antibodies, $CD4^+$ and $CD8^+$ T cells and a panel of 11 murine Th1, Th2 and Th17 cytokines. After *M. ulcerans* challenge, mice vaccinated with ER alone or ER + R_4Pam_2Cys were found to exhibit significantly more ER-specific antibodies than the other treatment groups (Fig 4A) despite not being fully protected. This indicates that, even though the ER protein is highly immunogenic, anti-ER antibodies do not appear to play a major role in controlling infection.

We next investigated if there were any differences in the ability of T cells harvested from the spleens of vaccinated mice to produce cytokines following stimulation with recombinant ER protein (Supplementary Table S1). Our results showed that the numbers of IFN-γ producing $CD4^+$ T cells across all vaccine groups did not differ, and in some cases, were higher in unvaccinated mice compared to those vaccinated with ER + R_4Pam_2Cys vaccine group (Fig 4B) indicating that there was no clear correlation between the frequencies of these cells and protection. Similarly, there also did not appear to be any correlation between TNF-α^+ $CD4^+$ T cells, IFN-γ^+ $CD8^+$ T cells or TNF-α^+ $CD8^+$ T cells and protection (Supplementary Table S1).

Comparing levels of cytokine production between vaccine groups also did not clearly identify any cytokines that correlated with protection (see Supplementary Table S1). For example, higher levels of TNF-α were present in the spleens of unvaccinated mice than BCG vaccinated mice (Fig 4C) and even though BCG vaccination resulted in significantly more IFN-γ in draining lymph nodes compared to unvaccinated mice, this was not observed for ER + R_4Pam_2Cys vaccinated mice (Fig 4D).

We therefore based our analysis on comparisons between diseased or protected mice irrespective of the vaccines they received (Fig. 4E,F). Herein, we identified significant increases of IL-2, IL-6, IL-10 IL-17A, IFN-γ, MIP-1b, TNF-α in the lymph nodes of protected mice (Fig. 4F) and significant increases of IFN-γ, IL-6, and TNF-α in the spleens of diseased mice (Fig. 4E). While these data implicate these cytokines as correlates of protection and disease, it did not rank the importance of each cytokine towards either outcome.

Identifying immune responses that predict vaccination outcome

To identify the immune parameters (features) that associate with the response variable 'vaccine protection' (here measured as time to reach our bioluminescence detection threshold) independent

of the vaccine used, we conducted a univariate regression analysis using the Cox proportional hazards model. We used this model as it accounts for the fact that a subset of mice (observations) was right-censored, as vaccination outcomes were not measured after 24 weeks post challenge. For each of the 28 immunological features, their association with the response variable (time-to-bioluminescence measured in weeks) was ranked using concordance index (CI) scores. The CI is analogous to the area under the ROC curve, with a CI value of 0.5 indicating a random correlation and 1 indicating a perfect, positive correlation (62). The CI for each univariate regression analysis was used to rank the strength of association for each of the 28 features against the response variable. Using a CI cut-off of 0.70, the top six features were identified as well as the direction of their association with prevention of development of bioluminescence (Table 2). Low levels of IFN-γ and high levels of IL-2 produced in mouse splenocytes were the top two immune parameter features influencing this model, reflected in the individual correlation between their respective titres and time-to-bioluminescence (Fig. 5A, B).

Next, using these top six features, we performed unsupervised machine learning to reveal any structure without the influence of labels, such as arbitrarily imposed bioluminescence thresholds. Here, the data separated into two main clusters. K-means clustering was then applied to assign mice (observations) to the two cluster groups. Inspection of the resulting cluster membership with respect to time to bioluminescence showed a separation of the mice either side of 17 weeks post *M. ulcerans* challenge (Fig. 5C).

Given that the clusters identified through unsupervised learning closely resembled a temporal breakpoint at 17 weeks, we further investigated this binary divide in the data. We used multivariate logistic regression and developed a low-error classifier that could generalize to unseen data, using the underlying structure apparent in the immunological data. We then tested the classifier through

extensive cross-validation. Observations (mice) with bioluminescence above threshold between weeks 8-17 were assigned a '0' and '1' for those with bioluminescence detected in weeks 18-24 or no detection throughout the experiment period. The model included the top six features (Table 2) and was validated through 1,000 random train test splits, with 90% of observations comprising the training groups at each split. The resulting classifier probabilities were used to calculate the area under the ROC curve, AUC = 0.91 (True negatives = 1774, True positives = 2662, False negatives = 120, False positives = 444). The low error and generalizable nature of this classifier demonstrates the existence of a robust structure in the data, in the form of two clusters separated around week 17 (Fig. 5D) and highlights the strong association of the six identified immune parameters with outcome. Most notably here it appears that tissue specific immune responses are important, with a correlation between the appearance of a tail ulcer and evidence of a systemic (spleen) responses and protection correlating with both local (draining lymph nodes) and systemic (spleen) response (Table 2). This association of BU and the production of inflammatory cytokines (IL-6, IFN-γ and TNF) as possible markers of infection, indicated that we could also identify correlates of immune protection against BU.

Assessment of vaccine-specific immune responses

To dissect the immune responses associated with ER + R_4Pam_2Cys vaccination versus BCG and the different controls we noted the differences in the percentage of observations (mice) belonging to specific treatment groups between the two clusters observed above (Fig. 5C) separated by week 17. This summary was reflective of the survival analysis and showed that unvaccinated mice and those that received the adjuvant or ER alone were predominantly in the weeks 8-17 cluster, while ER + R_4Pam_2Cys and BCG-vaccinated mice were predominantly in the weeks 18-24 cluster (Fig. 5E). In order to obtain the individual immune profile of the different treatment groups, group-specific univariate logistic regression analyses were undertaken. Here, the response variable was coded as

a '1' for membership in a particular group and '0' for membership in all other groups. Analyses were conducted for each of the five treatment groups and the model coefficient weights were used to determine both the strength and direction of association of each feature with that of each treatment group. The resulting *p*-values from the model coefficients were used to assess significance of the associations (Fig. 5F, Supplementary Table S2). The combination of the ER antigen and R_4Pam_2Cys together were important for inducing protective responses that associated with local production of IL-4, IL-2, IL-17A in the DLN, in addition to ER-specific antibody responses. Neither ER antigen or R_4Pam_2Cys alone induced this profile and protection using the former was only linked to ER- but not *M. ulcerans*-specific antibody responses (post-challenge timepoints). In comparison, BCG vaccination-mediated protection was associated with a greater breadth of localised cytokines responses than ER + R_4Pam_2Cys, with higher IL-6, TNF-α and MIP-1β in the DLN. Of note, evidence of systemic inflammation, such as IL-17A and IFN-γ in the spleen was associated with poorer BCG performance.

Discussion

In this study, we investigated various immune parameters induced by the use of BCG and an experimental subunit vaccine against BU and sought to identify immune correlates associated with protection in a mouse tail infection model. Studies have shown that the tail is a suitable location for infection as BU predominantly affects extremities (11, 52, 63) and in combination with the use of bioluminescent *M. ulcerans,* offers several advantages over footpad, hock or ear infections used in most BU vaccine studies (as shown in Table 1 and (64)). Tail infections are less likely to affect mouse mobility, or cause rapid tissue loss and may also prevent added trauma, inflammation or secondary infections at the challenge site (65). A key feature of this model also allows the use of a significantly lower bacterial challenge dose compared to other studies (approximately 14-20 CFU compared to 10^4-10^6 CFU) (25, 32-37, 49, 52-54) (Table 1) and enables measuring bacterial growth in the same

320 animal over time. This lower dose is likely to be more physiologically relevant, in terms of reflecting
321 the bacterial inoculum that occurs during *M. ulcerans* transmission to humans (10, 11, 59). Sporadic
322 healing of BU disease was also seen in this model, an observation that has been noted in humans
323 and other animals (29, 66-68).
324
325 Vaccination with the ER + R_4Pam_2Cys formulation resulted in protection of 60% of mice from BU
326 challenge. Although more of these vaccinated mice reached our defined disease outcome after 24
327 weeks compared to BCG-vaccinated mice, the difference was not statistically significant. There was
328 also no significant difference in the number of mice displaying any bioluminescence between each
329 group. The fact that ER + R_4Pam_2Cys was significantly more protective than vaccination with
330 R_4Pam_2Cys alone indicates any non-antigen specific triggering of innate immune responses by this
331 adjuvant (69, 70) (71) was not sufficient for conferring long-lasting protection and the inclusion of
332 the ER protein was necessary to achieve any protective effects. This was further evident by
333 vaccinating with ER alone. Despite not seeing any clear significant differences in the clinical
334 outcomes at the end of the trial when compared to ER + R_4Pam_2Cys vaccination, the inclusion of
335 R_4Pam_2Cys delayed disease onset by ~8 weeks and correlated with the induction of significantly
336 more ER-specific antibodies after a primary and booster vaccination.
337
338 The presence of these antibodies was nonetheless insufficient to provide total protection against
339 *M. ulcerans* challenge. This is perhaps not unexpected given that other studies have also reported
340 little correlation between strong BU antibodies and protection, in mice (34) or sera of BU patients
341 (57, 72). To identify other immune correlates associated with the protective effects observed in our
342 study, a Cox proportional hazards regression model was utilized. Here, the univariate analyses
343 allowed us to identify the top six features that most strongly associated with differences in time to
344 detection of bioluminescence. These models assume normalized data, and although we cannot infer

how much an increase or decrease in units could affect the clinical outcome, we are able to rank each factor based on its contribution to either disease or protection. This model also considers the effect of each factor in delaying the onset of disease rather than just modelling through a binary 'protected' or 'diseased' outcome. Similar regression modelling has been described to predict outcomes for tuberculosis patients after treatment, effect of hospital-acquired *Clostridium difficile* on hospital stay and survival of *Staphylococcus aureus* in milk (73-75). The model assumes that eventually all mice will succumb to disease and due to the constraints in our data, it cannot determine threshold levels of cytokines that will predict disease outcomes.

The cytokines most associated with protection in BCG mice were different to those identified in mice vaccinated with ER+R_4Pam_2Cys, which is not surprising given that BCG is a multi-antigen live-attenuated vaccine and thus likely to utilise both common and distinct protective responses and mechanisms to those induced by our vaccine candidate.

Through multivariate logistic regression modelling we identified the presence of IL-2 in the spleen and lymph nodes as markers that were most strongly associated with protection. Although there are no studies that directly link IL-2 with protection against *M. ulcerans*, it plays a key role in the differentiation, proliferation and maintenance of T cell responses (76). Therefore, it is perhaps not surprising that its role in this murine model is likely to be important for the induction of protective adaptive immunity against *M. ulcerans.*

However, our results did not show any correlation between levels of cytokine producing $CD4^+$ and $CD8^+$ T cells and protection in vaccinated groups despite studies that have shown them to play a role in BU control (77, 78). In particular, *M. ulcerans*-specific $CD4^+$ T cells have been found to migrate to the site of infection from draining lymph nodes early in infection but are depleted as the infection

persists (77), an effect that could be attributed to the ability of the *M. ulcerans* exotoxin mycolactone to impair T cell and macrophage function (41, 44, 78).

In addition, we also identified the presence of systemic IL-6, TNF-α and IFN-γ (in the spleen) to be strongly associated with disease. IL-6 is a pro-inflammatory cytokine produced by many cell types in response to pathogens and is linked to the production of TNF-α, both of which can be detected in BU lesions and serum of BU patients (78, 79) (80). TNF-α in particular, plays a key role in inflammatory cell recruitment and in conjunction with IFN-γ, increases the phagocytic ability of macrophages to enhance killing of mycobacteria (81, 82). However many studies have shown that mycolactone suppresses TNF-α production by T cells and especially macrophages (83, 84), decreasing their ability to control BU infection (85).

IFN-γ itself has also been shown to be important for controlling *M. ulcerans* infection as IFN-γ deficient mice cannot prevent the onset of disease (86). It is also detected at high levels in patients with both developed ulcers and early lesions (87) and healed ulcers (88) where it is believed to mediate macrophage function (89) and drive iNOS expression to facilitate bacterial killing (90). Altogether, the fact that these cytokines are elevated at a systemic level in the diseased animals in our study but not in lymph nodes draining from the tail suggests that their activity is being dampened at the site of infection. These effects do not appear to be present in protected animals where increased levels of cytokines are detected in the draining lymph node and not the spleen. In fact, the localised, but not systemic presence, of these and other cytokines including IL17A, MIP1b and IL10 are strongly associated with protection.

Although most of the immunosuppression during BU infection can be attributed to mycolactone, chronic inflammation can also be key driver as noted by the increased splenic cytokine levels. Many

395 cell types have been implicated as the cause of immunosuppression in cancers, chronic viral
396 infections (such as HCV, HIV, HBV) and even *M. tuberculosis* infection. These include myeloid-
397 derived suppressor cells (MDSCs) (91) regulatory T cells (T_{reg}) (92) and T helper 17 (T_h17) (93), which
398 can suppress effector T cell function and inhibit NK and dendritic cell activity through direct cell-to-
399 cell interactions or the production of immunosuppressive cytokines. MDSCs in particular can be
400 recruited by IFN-γ (94) and IL-6 (95), both of which are found in higher levels in our unprotected
401 mice. On the other hand, while T_h17 cells are crucial for the control of infection, especially
402 extracellular bacterial and fungal infections, elevated frequencies can lead to tissue inflammation
403 alongside matrix destruction, autoimmunity and vascular activation (96). The observation that
404 higher systemic IL-17A correlates with the lack of protection suggests that these cells play a role in
405 determining BU disease outcomes.
406
407 Tissue changes due to chronic infection could also play a compounding effect on the severity of BU
408 disease outcomes. Our histological analysis of BU-infected tail tissue showed a loss of muscle and
409 epidermis, changes in connective tissue and loss of vasculature which may explain why lymphocytes
410 and other immune cells are unable to access the sites of greatest infection and tissue damage. BU
411 tissue necrosis can also extend some distance from the site of bacterial colonisation, an observation
412 that led to the identification of mycolactone as the cause of coagulative necrosis (39, 97, 98).
413 Mycolactone has been well described as causing cell death to skin-resident cells such as fibroblasts,
414 adipocytes, keratinocytes and endothelial cells (39, 99, 100). Primary human dermal microvascular
415 endothelial cells are especially sensitive to mycolactone and after exposure lose their ability to
416 activate a key anticoagulant protein (protein C) after exposure, causing a reduction in intravascular
417 fluidity and preventing immune cell infiltration to the infection site (99). Thus, the combination of
418 immunosuppressive immune host responses and tissue destruction, in conjunction with

mycolactone at the site of infection, may increase the risk for poorer disease outcomes for those chronically infected with BU.

Although we have identified several factors associated with disease and protection, our results provide impetus to further expand these profiles and establish their importance. For example, changes in cytokines levels before challenge and throughout the infection phase could be monitored and integrated into models, as well as analysing frequencies of various other innate- and adaptive-immune cell populations and identifying those that produce cytokines of interest. In evaluating and demonstrating that a subunit vaccine can protect against BU in our mouse challenge model, albeit not as efficacious as BCG, our results showed that protection can be mediated through different immune mechanisms. Disease progression was also commonly linked to the presence of pro-inflammatory cytokines in the spleen and not the lymph node. These profiles indicate that localised and not systemic responses are more important for conferring protection and also provide a template that could guide the design and development of novel vaccination strategies against BU.

Finally, we conclude that the mycolactone biosynthesis pathway constitutes a viable vaccine target to protect against *M. ulcerans*. As *M. ulcerans* is slow-growing and requires its highly conserved mycolactone PKS for virulence, the development of resistance is unlikely. As such, approaches based on the use of multiple PKS enzymatic domains may prove even more efficacious. Moreover, studies that have introduced *M. ulcerans* and *M. marinum*-specific proteins into BCG have been shown to increase its protective effect. Collectively, this demonstrates the additive power of using a broader suite of antigens and the potential for a viable vaccine against BU.

Methods:

Strains and culture conditions.

444 *Escherichia coli* ClearColi©BL21 (DE3) containing the plasmid, pJexpress-ER (strain TPS847) was
445 grown at 37°C in Luria-Bertani (LB) broth (Difco, Becton Dickinson, MD, USA) supplemented with
446 100 µg/ml ampicillin (Sigma-Aldrich, USA) to express the enoyl reductase (ER) protein (57). Log-
447 phase bioluminescent *Mycobacterium ulcerans* (strain JKD8049 containing integrated plasmid
448 pMV306 *hsp:lux*G13) (10, 60) was grown at 30°C in 7H9 broth or 7H10 agar (Middlebrook, Becton
449 Dickinson, MD, USA) supplemented with oleic acid, albumin, dextrose and catalase growth
450 supplement (OADC) (Middlebrook, Becton Dickinson, MD, USA), 0.5% glycerol (v/v) and 25 µg/ml
451 kanamycin (Sigma-Aldrich, USA). *M. bovis* BCG (strain 'Danish 1331') used for vaccinations was
452 grown at 37°C in 7H9 broth or 7H10 agar supplemented with OADC. Mycobacterial colony counts
453 from cultures or tissue specimens were performed using spot plating as previously described (10).
454 All culture extracts were screened by LC-MS for the presence of mycolactones as previously
455 described to ensure bacteria used in transmission experiments remained fully virulent (101).
456
457 *Recombinant protein expression*
458 Overnight culture of *E. coli* TPS847 was diluted to OD_{600} = 0.05 in LB broth. The culture was incubated
459 at 37°C with shaking at 200 rpm until OD_{600} = 0.6-0.7, followed by the addition of 1 mM IPTG
460 (Isopropyl b-D-1-thiogalactopyr-anoside) to induce protein expression for a further four hours. Cells
461 were then resuspended in wash buffer (8 M urea, 150 mM sodium chloride, 10% glycerol) and
462 sonicated at amplitude 60 (QSonica Ultrasonic Liquid Processor S-4000, Misonix) until the solution
463 turned clear. The lysate was filtered with a 0.22 µM filter (Millipore) to remove cellular debris and
464 protein was column-purified using anti-histidine resin (ClonTech). The resin was washed with wash
465 buffer which was gradually replaced with tris buffer (20 mM Tris-HCl, 150 mM sodium chloride, 10%
466 glycerol) over ten washes followed by two washes with tris buffer containing 20 mM imidazole.
467 Protein was eluted in tris buffer containing 200 mM imidazole and dialysed in phosphate buffered
468 saline (PBS) before concentration using a microcon column (Millipore). Proteins were tested for

endotoxin contamination using Pierce™ limulus amoebocyte lysate assay (Thermo Scientific™) and relative size was confirmed by sodium dodecyl sulphate polyacrylamide gel electrophoresis.

Sodium dodecyl sulphate polyacrylamide gel electrophoresis (SDS-PAGE)

Samples were denatured in an equal volume of 2 x sample loading buffer (40% (v/v) 0.5M Tris-HCL pH6.8, 10% glycerol, 1.7% (w/v) SDS, 10% 2-B-mercaptoethanol, 0.13% (w/v) bromophenol blue in distilled water) at 100°C for 5 minutes. Ten microlitres of each sample and SeeBlue® Plus2 pre-stained protein standard (Invitrogen) was loaded onto a 0.5mm 12% polyacrylamide gel under reducing conditions, as previously described (102). The gel was run in buffer containing 0.3% (w/v) Tris, 1.44% (w/v) glycine and 0.1% (w/v) SDS in distilled water for 1 hour at 150 volts (Mini-protean vertical electrophoresis cell, Bio-Rad), stained in Coomassie stain (45% methanol, 10% acetic acid 0.25% (w/v) Coomassie brilliant blue in distilled water) for 1 hour and destained in Coomassie destain (33% Methanol, 10% acetic acid, 60% distilled water) until protein bands were visualised.

Western Blotting

Protein separated on a 12% polyacrylamide gel was transferred to a nitrocellulose membrane in a tris-glycine transfer buffer (1.5 mM Tris, 12mM glycine, 15 % methanol (v/v) in distilled water) for 1 hour at 100 volts (Mini Trans-Blot Cell, Bio-Rad) and incubated in blocking buffer (5% (w/v) skim milk powder and 0.1% Tween-20 in PBS) overnight at 4°C. The membrane was then incubated with anti6xHIS-HRP antibody (Roche Applied Science, USA) at 1:500 dilution for 2 hours and washed in PBS containing 0.1% Tween-20 prior to exposure to developing solution (Western Lighting Chemiluminescence kit, Perkin Elmer, USA) according to the manufacturer's guidelines. Chemiluminescence was detected using an MF ChemiBIS gel imaging system (DNR Bio-Imaging Systems, Israel).

494 *Particle size analysis of protein antigen and lipopeptide formulations by dynamic light scattering*
495 *(DLS)*

496 The association between protein and R_4Pam_2Cys was measured using dynamic light scattering (DLS)
497 by mixing 5 µg of protein with increasing amounts of lipopeptide in 50 µl PBS. The size distribution
498 of particles in solution (presented as hydrodynamic radius) were measured in 4µl of cyclin olefin co-
499 polymer cuvettes using a DynaPro NanoStar DLS instrument (Wyatt Technology, CA, USA) equipped
500 with 658nm laser with a scattering angle of 90°. Measurements were acquired in triplicate with each
501 measurement consisting of 30 readings at 5 second intervals at 25°C. Data was analysed using
502 Dynamics software (v7.1.7.16).

503

504 *Vaccination of animals*

505 The synthesis and purification of the branched cationic lipopeptide, R_4Pam_2Cys, was performed as
506 previously described (103, 104). Each vaccine dose contained 25 µg protein formulated in PBS with
507 R_4Pam_2Cys at a 1:5 molar ratio of protein to lipopeptide in a final volume of 100 µl. Live-attenuated
508 *M. bovis* BCG strain 'Danish 1331' was grown to log phase and stored at -80°C in 20% glycerol until
509 used. Bacteria were washed with PBS and resuspended in 200ul, before administration at 4.7×10^5
510 bacteria per dose. All vaccines and control formulations were sonicated for 5 minutes in a waterbath
511 sonicator before being administered.

512

513 Female 6-week old BALB/c mice were sourced from ARC (Canning Vale, Australia) and housed in
514 individual ventilated cages. Food and water were given *ad libitum*. Experiments were approved by
515 The University of Melbourne Animal Ethics Committee (Approval identification number: 1613870).
516 For vaccination using R_4Pam_2Cys, animals were inoculated subcutaneously at the base of tail (100µl
517 per dose at 50 µl per flank) and boosted 21 days later with the same formulations. Mice vaccinated

518 with *M. bovis* BCG were given one dose subcutaneously in a similar manner (200 µl per dose at 100µl
519 per flank). There were 10 mice in each vaccination group.
520
521 *M. ulcerans challenge*
522 Mice were challenged with bioluminescent *M. ulcerans* on day 35 as described previously (10).
523 Briefly, tails of isoflurane anaesthetised mice were dipped in 7H9 culture containing log-phase
524 bioluminescent *M. ulcerans* bacteria (concentration 1.27 x 10^6 CFU/mL (range: 1.07x10^6 – 1.46 x10^6
525 CFU). Contaminated tails were then pierced once subcutaneously with a sterile 25-G needle. The
526 infectious dose was calculated to be 17 CFU (range: 14-20) using methods previously described (10).
527 Mice were allowed to recover and monitored for up to 24 weeks after infection and sacrificed when
528 tail ulceration was observed wherein spleens, lymph nodes and sera were harvested for
529 immunological analysis.
530
531 *IVIS imaging*
532 Infected mice were imaged weekly from 6-weeks post-infection to detect the emission of
533 bioluminescence. Images were captured using the Lumina XRS Series III In Vitro Imaging System
534 (IVIS®) (Perkin Elmer, MA, USA) and Living Image Software v3.2 with the following settings: Field of
535 View 24, relative aperture f'1.2, medium binning, 60s exposure. Bioluminescence was calculated
536 using Living Image Software v3.2.
537
538 *Serum antibody titre measurements*
539 Serum antibody titres were measured by enzyme linked immunosorbent assay (ELISA) (105) using
540 plates (Nunc, Thermo Scientific) that were previously coated with antigen overnight, either purified
541 recombinant ER protein or heat-killed whole cell *M. ulcerans* lysate. The presence of bound
542 antibodies were detected by incubating serum-exposed wells with horse radish peroxidase

543 conjugated rabbit anti-mouse IgG (Dako, Glostrup, Denmark) for 2 hours followed by the addition
544 of the enzyme substrate (0.2mM ABTS in 50mM citric acid containing 0.004% hydrogen peroxide
545 and left to develop for 10-15 minutes before the addition of 50nM sodium fluoride to stop the
546 reaction. Plates were read at dual wavelengths of 505 and 595 nm on plate reader (LabSystems
547 Multiskan Multisoft microplate reader) and antibody titres expressed as the reciprocal of the
548 highest dilution of serum required to achieve an optical density of 0.2.
549
550 *Intracellular cytokine staining*
551 Single cell suspensions were derived from the spleen and draining lymph nodes and resuspended in
552 RP10 media (RPMI 1640 (Sigma) supplemented with 10% foetal bovine serum (Gibco, ThermoFisher
553 Scientific, Waltham, MA USA), 2mM L-glutamine, 1mM sodium pyruvate, 55 µM 2-
554 mercaptoethanol, 12 µg gentamycin, 100 U/ml penicillin and 100 µg/ml streptomycin). Spleen and
555 lymph node-derived cells were cultured in 96-well plates (CoStar, Corning, USA) at 1 x10^7 cells/per
556 well and 1 x10^5 cells/well, respectively 200 µl of RP10 containing 10 U/ml IL-2 (Roche, Mannheim,
557 Germany), 1µg/ml plate-bound anti-CD28 (BD Pharmingen, Becton Dickinson, Clone 37.51) and 20
558 µg/ml ER protein for 12 hours at 37°C in 5% CO_2. Golgiplug (1µg/ml) (Becton Dickinson) was added
559 for the last 4 hours of incubation. Cells were then stained with 7AAD-Live/Dead stain dye (Biolegend,
560 CA, USA), BV510-anti-B220 (BD Horizon, Becton Dickinson, Clone RA3-6B2), BV605-antiCD4
561 (Biolegend, Clone RM4-5), APC-Cy7-anti-TCRb (BD Pharmingen, Clone H57-597) and PE-Cy7-anti-
562 CD8 (BD Pharmingen, Clone 53-6.7) anti-mouse monoclonal antibodies at 4°C in the dark.
563 Intracellular staining was performed by fixing cells with Cytofix/Cytoperm solution (Becton
564 Dickinson, USA) followed by permeabilisation and intracellular staining with Perm/Wash buffer
565 (Becton Dickinson) and BV786-IFN-γ (BD Horizon, Clone XM G1.2), AF647-IL-17A (BD Pharmingen,
566 Becton Dickinson, Clone TCII-18H10) and PE-TNF-α (BD Biosciences, Clone MP6-XT22) antibodies

567 for 30 minutes at 4°C before analysis on an LSR Fortessa flow cytometer (BD Biosciences, US). Data
568 analyses were performed using FlowJo (Tree Star, OR, USA).
569
570 *Cytokine Bead Array*
571 Spleen and lymph node-derived cells were incubated in 500 µl RP10 supplemented with 25 µg/ml
572 ER protein for 72 hours at 37°C in 5% CO_2. Supernatant was collected and a cytokine bead array was
573 performed using a mouse flex set (BD Biosciences, USA) to detect IL-2, IL-4, IL-6, IL-10, IL-12/IL-
574 23p40, IL-17, IFN-γ, TNF, MCP-1, MIP1α, MIP1β as per the manufacturer's instructions. Samples
575 were acquired using a FACSCanto II flow cytometer (BD Biosciences) and cytokine quantities
576 calculated using FCAP Array™ Software v3.0.
577
578 *Histology and microscopy*
579 Tail tissues from the site of infection were fixed in PBS containing 10% non-buffered formalin then
580 embedded in paraffin and sliced into 10 µM thick segments. The sliced segments were Ziehl
581 Neelsen- or H&E-stained prior to microscope imaging. Images of tail segments were captured using
582 a light microscope (Olympus BX53 Light microscope, Olympus-Life Science).
583
584 *Statistical analysis*
585 GraphPad Prism software (GraphPad Software v7, CA, USA) was used to perform statistical analyses
586 on the antibody titre, time to luminescence, T cell numbers and cytokine titre data. Antibody titres
587 were analysed using one-way ANOVA with Tukey's correction for multiple comparisons. The time to
588 bioluminescence data was displayed as a Kaplan-Meier plot and differences determined using a Log-
589 Rank (Mantel-Cox) test. Mann-Whitney tests were performed to compare cytokine titres between
590 protected and diseased mice and for comparisons between vaccination groups. All tests were
591 conducted at the 5% significance level.

Statistical modelling

Twenty-eight data features (*i.e.* the immune parameters measured in each mouse, refer to Table S1) were transformed using the R package *bestNormalize* (106). Transformed features were then normalised (between 0 and 1 for each feature) using the *MinMaxScaler* function of *Scikit-learn* (107). As many of the vaccination outcome observations (time-to-bioluminescence) were right-censored, we employed the Cox proportional hazards regression analysis using the *Scikit-survival* module of *Scikit-learn* in Python (108). Here, univariate analyses were run for each of the 28 features using the continuous response variable of time-to-bioluminescence. The standard metric for assessing the predictive performance of a survival model is the concordance index (CI) (62, 109, 110). A CI >0.7 was used to identify the top six features of this model. Unsupervised learning and data dimensionality reduction is an ideal way to identify structure in continuous data without the influence of labels. The method of *t-Distributed Stochastic Neighbor Embedding* (t-SNE) is a dimensionality reduction technique that retains both the global structure and local layout of the high-dimensional data through exchanging the Euclidean distances between all pair of data points into heavy-tailed conditional probabilities (111). This method is advantageous over conventional principal component analysis (PCA), as it does not rely on a linear assumption and can capture nonlinear relationships (111). We explored the data, independent of labels, by reducing the top six features obtained from the Cox proportional hazards regression analysis to a two-dimensional space using the t-SNE package in *Scikit-learn* (107) . The two clusters detected through visual inspection were objectively defined, with observations assigned to two groups using K-means clustering, as implemented in *Scikit-learn* (107). A multivariate logistic regression classifier was then built using the top six features, with the two clusters identified by *t-SNE* as the response variables. To reduce the possibility of over-fitting, the model was validated through 1,000 random train-test splits, in which 90% of the observations made up each training set. These models were built using the logistic

617 regression classifier as implemented in *Scikit-learn* (107) and Receiver-Operator-Characteristic
618 curves were used to evaluate model performance (112). In order to assess the immune features
619 that were associated with different vaccination groups, a univariate logistic regression analysis was
620 then conducted for each group using *R* (112). The estimated model coefficients were used to assess
621 the direction and strength of the association, and the corresponding p-value used to determine
622 statistical significance at the 5% significance level.

Acknowledgments: We thank Laura Leone for expert assistance with histology. This research was supported by the National Health and Medical Research Council, Australia (GNT1008549). The funders had no role in study design, data collection and interpretation, or the decision to submit the work for publication.

References:

1. Guarner J, Bartlett J, Whitney EA, Raghunathan PL, Stienstra Y, Asamoa K, Etuaful S, Klutse E, Quarshie E, van der Werf TS, van der Graaf WT, King CH, Ashford DA. 2003. Histopathologic features of *Mycobacterium ulcerans* infection. Emerg Infect Dis 9:651-656.
2. Vincent QB, Ardant MF, Adeye A, Goundote A, Saint-Andre JP, Cottin J, Kempf M, Agossadou D, Johnson C, Abel L, Marsollier L, Chauty A, Alcais A. 2014. Clinical epidemiology of laboratory-confirmed Buruli ulcer in Benin: a cohort study. Lancet Glob Health 2:e422-30.
3. Hayman J, McQueen A. 1985. The pathology of *Mycobacterium ulcerans* infection. Pathology 17:594-600.
4. Oliveira MS, Fraga AG, Torrado E, Castro AG, Pereira JP, Filho AL, Milanezi F, Schmitt FC, Meyers WM, Portaels F, Silva MT, Pedrosa J. 2005. Infection with *Mycobacterium ulcerans* induces persistent inflammatory responses in mice. Infect Immun 73:6299-310.
5. Yerramilli A, Tay EL, Stewardson AJ, Kelley PG, Bishop E, Jenkin GA, Starr M, Trevillyan J, Hughes A, Friedman ND, O'Brien DP, Johnson PDR. 2017. The location of Australian Buruli ulcer lesions-Implications for unravelling disease transmission. PLoS Negl Trop Dis 11:e0005800.
6. van der Werf TS, van der Graaf WT, Tappero JW, Asiedu K. 1999. *Mycobacterium ulcerans* infection. Lancet 354:1013-8.
7. Pszolla N, Sarkar MR, Strecker W, Kern P, Kinzl L, Meyers WM, Portaels F. 2003. Buruli ulcer: a systemic disease. Clin Infect Dis 37:e78-82.
8. Loftus MJ, Tay EL, Globan M, Lavender CJ, Crouch SR, Johnson PDR, Fyfe JAM. 2018. Epidemiology of Buruli Ulcer Infections, Victoria, Australia, 2011-2016. Emerg Infect Dis 24:1988-1997.
9. Toll A, Gallardo F, Ferran M, Gilaberte M, Iglesias M, Gimeno JL, Rondini S, Pujol RM. 2005. Aggressive multifocal Buruli ulcer with associated osteomyelitis in an HIV-positive patient. Clin Exp Dermatol 30:649-51.
10. Wallace JR, Mangas KM, Porter JL, Marcsisin R, Pidot SJ, Howden B, Omansen TF, Zeng W, Axford JK, Johnson PDR, Stinear TP. 2017. Mycobacterium ulcerans low infectious dose and mechanical transmission support insect bites and puncturing injuries in the spread of Buruli ulcer. PLoS Negl Trop Dis 11:e0005553.
11. Marsollier L, Robert R, Aubry J, Saint Andre JP, Kouakou H, Legras P, Manceau AL, Mahaza C, Carbonnelle B. 2002. Aquatic insects as a vector for *Mycobacterium ulcerans*. Appl Environ Microbiol 68:4623-8.
12. Meyers WM, Shelly WM, Connor DH, Meyers EK. 1974. Human *Mycobacterium ulcerans* infections developing at sites of trauma to skin. Am J Trop Med Hyg 23:919-23.

13. Buultjens AH, Vandelannoote K, Meehan CJ, Eddyani M, de Jong BC, Fyfe JAM, Globan M, Tobias NJ, Porter JL, Tomita T, Tay EL, Seemann T, Howden BP, Johnson PDR, Stinear TP. 2018. Comparative Genomics Shows That *Mycobacterium ulcerans* Migration and Expansion Preceded the Rise of Buruli Ulcer in Southeastern Australia. Appl Environ Microbiol 84.
14. Simpson H, Deribe K, Tabah EN, Peters A, Maman I, Frimpong M, Ampadu E, Phillips R, Saunderson P, Pullan RL, Cano J. 2019. Mapping the global distribution of Buruli ulcer: a systematic review with evidence consensus. Lancet Glob Health 7:e912-e922.
15. Stinear TP, Seemann T, Pidot S, Frigui W, Reysset G, Garnier T, Meurice G, Simon D, Bouchier C, Ma L, Tichit M, Porter JL, Ryan J, Johnson PD, Davies JK, Jenkin GA, Small PL, Jones LM, Tekaia F, Laval F, Daffe M, Parkhill J, Cole ST. 2007. Reductive evolution and niche adaptation inferred from the genome of *Mycobacterium ulcerans*, the causative agent of Buruli ulcer. Genome Res 17:192-200.
16. Marsollier L, Stinear T, Aubry J, Saint Andre JP, Robert R, Legras P, Manceau AL, Audrain C, Bourdon S, Kouakou H, Carbonnelle B. 2004. Aquatic plants stimulate the growth of and biofilm formation by *Mycobacterium ulcerans* in axenic culture and harbor these bacteria in the environment. Appl Environ Microbiol 70:1097-103.
17. Loftus MJ, Trubiano JA, Tay EL, Lavender CJ, Globan M, Fyfe JAM, Johnson PDR. 2018. The incubation period of Buruli ulcer (*Mycobacterium ulcerans* infection) in Victoria, Australia - Remains similar despite changing geographic distribution of disease. PLoS Negl Trop Dis 12:e0006323.
18. Trubiano JA, Lavender CJ, Fyfe JA, Bittmann S, Johnson PD. 2013. The incubation period of Buruli ulcer (*Mycobacterium ulcerans* infection). PLoS Negl Trop Dis 7:e2463.
19. Sarfo FS, Phillips R, Asiedu K, Ampadu E, Bobi N, Adentwe E, Lartey A, Tetteh I, Wansbrough-Jones M. 2010. Clinical efficacy of combination of rifampin and streptomycin for treatment of *Mycobacterium ulcerans* disease. Antimicrob Agents Chemother 54:3678-85.
20. Nienhuis WA, Stienstra Y, Thompson WA, Awuah PC, Abass KM, Tuah W, Awua-Boateng NY, Ampadu EO, Siegmund V, Schouten JP, Adjei O, Bretzel G, van der Werf TS. 2010. Antimicrobial treatment for early, limited *Mycobacterium ulcerans* infection: a randomised controlled trial. Lancet 375:664-72.
21. Wadagni AC, Barogui YT, Johnson RC, Sopoh GE, Affolabi D, van der Werf TS, de Zeeuw J, Kleinnijenhuis J, Stienstra Y. 2018. Delayed versus standard assessment for excision surgery in patients with Buruli ulcer in Benin: a randomised controlled trial. Lancet Infect Dis 18:650-656.
22. Zingue D, Bouam A, Tian RBD, Drancourt M. 2018. Buruli Ulcer, a Prototype for Ecosystem-Related Infection, Caused by Mycobacterium ulcerans. Clin Microbiol Rev 31.
23. Tanghe A, Adnet PY, Gartner T, Huygen K. 2007. A booster vaccination with Mycobacterium bovis BCG does not increase the protective effect of the vaccine against experimental *Mycobacterium ulcerans* infection in mice. Infect Immun 75:2642-4.
24. Converse PJ, Almeida DV, Nuermberger EL, Grosset JH. 2011. BCG-mediated protection against *Mycobacterium ulcerans* infection in the mouse. PLoS Negl Trop Dis 5:e985.
25. Fraga AG, Martins TG, Torrado E, Huygen K, Portaels F, Silva MT, Castro AG, Pedrosa J. 2012. Cellular immunity confers transient protection in experimental Buruli ulcer following BCG or mycolactone-negative *Mycobacterium ulcerans* vaccination. PLoS One 7:e33406.
26. Walsh DS, Dela Cruz EC, Abalos RM, Tan EV, Walsh GP, Portaels F, Meyers WM. 2007. Clinical and histologic features of skin lesions in a cynomolgus monkey experimentally infected with *Mycobacterium ulcerans* (Buruli ulcer) by intradermal inoculation. Am J Trop Med Hyg 76:132-4.

27. Ortiz RH, Leon DA, Estevez HO, Martin A, Herrera JL, Romo LF, Portaels F, Pando RH. 2009. Differences in virulence and immune response induced in a murine model by isolates of *Mycobacterium ulcerans* from different geographic areas. Clin Exp Immunol 157:271-81.
28. Bolz M, Ruggli N, Ruf MT, Ricklin ME, Zimmer G, Pluschke G. Experimental infection of the pig with Mycobacterium ulcerans: a novel model for studying the pathogenesis of Buruli ulcer disease.
29. Marion E, Jarry UA-Ohoo, Cano C, Savary CA-Ohoo, Beauvillain CA-Ohoo, Robbe-Saule M, Preisser L, Altare F, Delneste Y, Jeannin P, Marsollier L. FVB/N Mice Spontaneously Heal Ulcerative Lesions Induced by Mycobacterium ulcerans and Switch M. ulcerans into a Low Mycolactone Producer.
30. Benard AA-OhooX, Sala C, Pluschke G. Mycobacterium ulcerans Mouse Model Refinement for Pre-Clinical Profiling of Vaccine Candidates.
31. Walsh DS, Meyers Wm Fau - Krieg RE, Krieg Re Fau - Walsh GP, Walsh GP. Transmission of Mycobacterium ulcerans to the nine-banded armadillo.
32. Tanghe A, Content J, Van Vooren JP, Portaels F, Huygen K. 2001. Protective efficacy of a DNA vaccine encoding antigen 85A from Mycobacterium bovis BCG against Buruli ulcer. Infect Immun 69:5403-11.
33. Tanghe A, Dangy JP, Pluschke G, Huygen K. 2008. Improved protective efficacy of a species-specific DNA vaccine encoding mycolyl-transferase Ag85A from *Mycobacterium ulcerans* by homologous protein boosting. PLoS Negl Trop Dis 2:e199.
34. Bolz M, Benard A, Dreyer AM, Kerber S, Vettiger A, Oehlmann W, Singh M, Duthie MS, Pluschke G. 2016. Vaccination with the Surface Proteins MUL_2232 and MUL_3720 of Mycobacterium ulcerans Induces Antibodies but Fails to Provide Protection against Buruli Ulcer. PLoS Negl Trop Dis 10:e0004431.
35. Hart BE, Hale LP, Lee S. 2016. Immunogenicity and protection conferred by a recombinant Mycobacterium marinum vaccine against Buruli ulcer. Trials in Vaccinology 5:88-91.
36. Hart BE, Hale LP, Lee S. 2015. Recombinant BCG Expressing Mycobacterium ulcerans Ag85A Imparts Enhanced Protection against Experimental Buruli ulcer. PLoS Negl Trop Dis 9:e0004046.
37. Hart BE, Lee S. 2016. Overexpression of a Mycobacterium ulcerans Ag85B-EsxH Fusion Protein in Recombinant BCG Improves Experimental Buruli Ulcer Vaccine Efficacy. PLoS Negl Trop Dis 10:e0005229.
38. Gowthaman U, Mushtaq K, Tan AC, Rai PK, Jackson DC, Agrewala JN. 2015. Challenges and solutions for a rational vaccine design for TB-endemic regions. Crit Rev Microbiol 41:389-98.
39. George KM, Chatterjee D, Gunawardana G, Welty D, Hayman J, Lee R, Small PL. 1999. Mycolactone: a polyketide toxin from *Mycobacterium ulcerans* required for virulence. Science 283:854-7.
40. Ogbechi J, Hall BS, Sbarrato T, Taunton J, Willis AE, Wek RC, Simmonds RE. 2018. Inhibition of Sec61-dependent translocation by mycolactone uncouples the integrated stress response from ER stress, driving cytotoxicity via translational activation of ATF4. Cell Death & Disease 9:397.
41. Baron L, Paatero AO, Morel JD, Impens F, Guenin-Mace L, Saint-Auret S, Blanchard N, Dillmann R, Niang F, Pellegrini S, Taunton J, Paavilainen VO, Demangel C. 2016. Mycolactone subverts immunity by selectively blocking the Sec61 translocon. J Exp Med 213:2885-2896.
42. Coutanceau E, Decalf J, Martino A, Babon A, Winter N, Cole ST, Albert ML, Demangel C. 2007. Selective suppression of dendritic cell functions by *Mycobacterium ulcerans* toxin mycolactone. J Exp Med 204:1395-403.

763 43. Meier JL, Burkart MD. 2011. Proteomic analysis of polyketide and nonribosomal peptide
764 biosynthesis. Curr Opin Chem Biol 15:48-56.
765 44. Boulkroun S, Guenin-Mace L, Thoulouze MI, Monot M, Merckx A, Langsley G, Bismuth G, Di
766 Bartolo V, Demangel C. 2010. Mycolactone suppresses T cell responsiveness by altering
767 both early signaling and posttranslational events. J Immunol 184:1436-44.
768 45. Pahlevan AA, Wright DJ, Andrews C, George KM, Small PL, Foxwell BM. 1999. The inhibitory
769 action of *Mycobacterium ulcerans* soluble factor on monocyte/T cell cytokine production
770 and NF-kappa B function. J Immunol 163:3928-35.
771 46. Torrado E, Fraga AG, Logarinho E, Martins TG, Carmona JA, Gama JB, Carvalho MA, Proença
772 F, Castro AG, Pedrosa J. 2010. IFN-γ–Dependent Activation of Macrophages during
773 Experimental Infections by Mycobacterium ulcerans Is Impaired by
774 the Toxin Mycolactone. The Journal of Immunology 184:947.
775 47. Stinear TP, Mve-Obiang A, Small PL, Frigui W, Pryor MJ, Brosch R, Jenkin GA, Johnson PD,
776 Davies JK, Lee RE, Adusumilli S, Garnier T, Haydock SF, Leadlay PF, Cole ST. 2004. Giant
777 plasmid-encoded polyketide synthases produce the macrolide toxin of *Mycobacterium*
778 *ulcerans*. Proc Natl Acad Sci U S A 101:1345-9.
779 48. Stinear TP, Pryor MJ, Porter JL, Cole ST. 2005. Functional analysis and annotation of the
780 virulence plasmid pMUM001 from *Mycobacterium ulcerans*. Microbiology 151:683-92.
781 49. Roupie V, Pidot SJ, Einarsdottir T, Van Den Poel C, Jurion F, Stinear TP, Huygen K. 2014.
782 Analysis of the vaccine potential of plasmid DNA encoding nine mycolactone polyketide
783 synthase domains in *Mycobacterium ulcerans* infected mice. PLoS Negl Trop Dis 8:e2604.
784 50. Chua BY, Zeng W, Jackson DC. 2008. Synthesis of toll-like receptor-2 targeting lipopeptides
785 as self-adjuvanting vaccines. Methods Mol Biol 494:247-61.
786 51. Wang Z, Kedzierski L, Nuessing S, Chua BY, Quinones-Parra SM, Huber VC, Jackson DC,
787 Thomas PG, Kedzierska K. 2016. Establishment of memory CD8+ T cells with live attenuated
788 influenza virus across different vaccination doses. J Gen Virol 97:3205-3214.
789 52. Coutanceau E, Legras P, Marsollier L, Reysset G, Cole ST, Demangel C. 2006.
790 Immunogenicity of *Mycobacterium ulcerans* Hsp65 and protective efficacy of a
791 *Mycobacterium leprae* Hsp65-based DNA vaccine against Buruli ulcer. Microbes Infect
792 8:2075-81.
793 53. Trigo G, Martins TG, Fraga AG, Longatto-Filho A, Castro AG, Azeredo J, Pedrosa J. 2013.
794 Phage therapy is effective against infection by *Mycobacterium ulcerans* in a murine
795 footpad model. PLoS Negl Trop Dis 7:e2183.
796 54. Watanabe M, Nakamura H, Nabekura R, Shinoda N, Suzuki E, Saito H. 2015. Protective
797 effect of a dewaxed whole-cell vaccine against Mycobacterium ulcerans infection in mice.
798 Vaccine 33:2232-9.
799 55. Dangy JP, Scherr N, Gersbach P, Hug MN, Bieri R, Bomio C, Li J, Huber S, Altmann KH,
800 Pluschke G. 2016. Antibody-Mediated Neutralization of the Exotoxin Mycolactone, the
801 Main Virulence Factor Produced by Mycobacterium ulcerans. PLoS Negl Trop Dis
802 10:e0004808.
803 56. Porter JL, Tobias NJ, Pidot SJ, Falgner S, Tuck KL, Vettiger A, Hong H, Leadlay PF, Stinear TP.
804 2013. The cell wall-associated mycolactone polyketide synthases are necessary but not
805 sufficient for mycolactone biosynthesis. PLoS One 8:e70520.
806 57. Pidot SJ, Porter JL, Marsollier L, Chauty A, Migot-Nabias F, Badaut C, Benard A, Ruf MT,
807 Seemann T, Johnson PD, Davies JK, Jenkin GA, Pluschke G, Stinear TP. 2010. Serological
808 evaluation of *Mycobacterium ulcerans* antigens identified by comparative genomics. PLoS
809 Negl Trop Dis 4:e872.

58. Pidot SJ, Hong H, Seemann T, Porter JL, Yip MJ, Men A, Johnson M, Wilson P, Davies JK, Leadlay PF, Stinear TP. 2008. Deciphering the genetic basis for polyketide variation among mycobacteria producing mycolactones. BMC Genomics 9:462.
59. Meyers Wm Fau - Shelly WM, Shelly Wm Fau - Connor DH, Connor Dh Fau - Meyers EK, Meyers EK. Human Mycobacterium ulcerans infections developing at sites of trauma to skin.
60. Omansen TF, Porter JL, Johnson PDR, van der Werf TS, Stienstra Y, Stinear TP. 2015. In-vitro Activity of Avermectins against Mycobacterium ulcerans. PLoS Neglected Tropical Diseases 9:e0003549.
61. Omansen TF, Marcsisin RA, Chua BY, Zeng W, Jackson DC, Porter JL, Stienstra Y, van der Werf TS, Stinear TP. 2019. In Vivo Imaging of Bioluminescent Mycobacterium ulcerans: A Tool to Refine the Murine Buruli Ulcer Tail Model. Am J Trop Med Hyg In Press.
62. Van Belle V, Pelckmans K, Van Huffel S, Suykens JA. 2011. Support vector methods for survival analysis: a comparison between ranking and regression approaches. Artif Intell Med 53:107-18.
63. Marion E, Jarry U, Cano C, Savary C, Beauvillain C, Robbe-Saule M, Preisser L, Altare F, Delneste Y, Jeannin P, Marsollier L. 2016. FVB/N Mice Spontaneously Heal Ulcerative Lesions Induced by Mycobacterium ulcerans and Switch M. ulcerans into a Low Mycolactone Producer. Journal of Immunology 196:2690-2698.
64. Bénard A, Sala C, Pluschke G. 2016. Mycobacterium ulcerans Mouse Model Refinement for Pre-Clinical Profiling of Vaccine Candidates. PLOS ONE 11:e0167059.
65. Kamala T. Hock immunization: a humane alternative to mouse footpad injections.
66. O'Brien DP, Murrie A, Meggyesy P, Priestley J, Rajcoomar A, Athan E. 2019. Spontaneous healing of Mycobacterium ulcerans disease in Australian patients. PLoS Negl Trop Dis 13:e0007178.
67. Marion E, Chauty A, Kempf M, Le Corre Y, Delneste Y, Croue A, Marsollier L. 2016. Clinical Features of Spontaneous Partial Healing During Mycobacterium ulcerans Infection. Open Forum Infect Dis 3:ofw013.
68. Silva-Gomes R, Marcq E, Trigo G, Gonçalves CM, Longatto-Filho A, Castro AG, Pedrosa J, Fraga AG. 2015. Spontaneous Healing of Mycobacterium ulcerans Lesions in the Guinea Pig Model. PLOS Neglected Tropical Diseases 9:e0004265.
69. Tan AC, Mifsud Ej Fau - Zeng W, Zeng W Fau - Edenborough K, Edenborough K Fau - McVernon J, McVernon J Fau - Brown LE, Brown Le Fau - Jackson DC, Jackson DC. Intranasal administration of the TLR2 agonist Pam2Cys provides rapid protection against influenza in mice.
70. Mifsud EJ, Tan AC, Reading PC, Jackson DC. Mapping the pulmonary environment of animals protected from virulent H1N1 influenza infection using the TLR-2 agonist Pam(2)Cys.
71. Mifsud EJ, Tan AC, Short KR, Brown LE, Chua BY, Jackson DC. Reducing the impact of influenza-associated secondary pneumococcal infections.
72. Gooding TM, Johnson PD, Campbell DE, Hayman JA, Hartland EL, Kemp AS, Robins-Browne RM. 2001. Immune response to infection with *Mycobacterium ulcerans*. Infect Immun 69:1704-7.
73. Tolosie K, Sharma MK. Application of cox proportional hazards model in case of tuberculosis patients in selected addis ababa health centres, ethiopia.
74. Cole Sr Fau - Hudgens MG, Hudgens MG. Survival analysis in infectious disease research: describing events in time.
75. Forster AJ, Taljaard M, Oake N, Wilson K, Roth V, van Walraven C. 2012. The effect of hospital-acquired infection with Clostridium difficile on length of stay in hospital. CMAJ :

Canadian Medical Association journal = journal de l'Association medicale canadienne 184:37-42.

76. Kalia V, Sarkar S. 2018. Regulation of Effector and Memory CD8 T Cell Differentiation by IL-2-A Balancing Act. Front Immunol 9:2987.

77. Fraga AG, Cruz A Fau - Martins TG, Martins Tg Fau - Torrado E, Torrado E Fau - Saraiva M, Saraiva M Fau - Pereira DR, Pereira Dr Fau - Meyers WM, Meyers Wm Fau - Portaels F, Portaels F Fau - Silva MT, Silva Mt Fau - Castro AG, Castro Ag Fau - Pedrosa J, Pedrosa J. Mycobacterium ulcerans triggers T-cell immunity followed by local and regional but not systemic immunosuppression.

78. Phillips R, Sarfo FS, Guenin-Mace L, Decalf J, Wansbrough-Jones M, Albert ML, Demangel C. 2009. Immunosuppressive signature of cutaneous *Mycobacterium ulcerans* infection in the peripheral blood of patients with buruli ulcer disease. J Infect Dis 200:1675-84.

79. Kiszewski AE, Becerril E, Aguilar LD, Kader IT, Myers W, Portaels F, Hernandez Pando R. 2006. The local immune response in ulcerative lesions of Buruli disease. Clin Exp Immunol 143:445-51.

80. Peduzzi E, Groeper C Fau - Schutte D, Schutte D Fau - Zajac P, Zajac P Fau - Rondini S, Rondini S Fau - Mensah-Quainoo E, Mensah-Quainoo E Fau - Spagnoli GC, Spagnoli Gc Fau - Pluschke G, Pluschke G Fau - Daubenberger CA, Daubenberger CA. Local activation of the innate immune system in Buruli ulcer lesions.

81. Ray JCJ, Wang J, Chan J, Kirschner DE. 2008. The timing of TNF and IFN-gamma signaling affects macrophage activation strategies during Mycobacterium tuberculosis infection. Journal of theoretical biology 252:24-38.

82. Cavalcanti YV, Brelaz MC, Neves JK, Ferraz JC, Pereira VR. 2012. Role of TNF-Alpha, IFN-Gamma, and IL-10 in the Development of Pulmonary Tuberculosis. Pulm Med 2012:745483.

83. Hall BS, Hill K, McKenna M, Ogbechi J, High S, Willis AE, Simmonds RE. 2014. The Pathogenic Mechanism of the Mycobacterium ulcerans Virulence Factor, Mycolactone, Depends on Blockade of Protein Translocation into the ER. PLOS Pathogens 10:e1004061.

84. Pahlevan AA, Wright DJM, Andrews C, George KM, Small PLC, Foxwell BM. 1999. The Inhibitory Action of Mycobacterium ulcerans Soluble Factor on Monocyte/T Cell Cytokine Production and NF-κB Function. J Immunol 163:3928.

85. Torrado E, Adusumilli S, Fraga AG, Small PLC, Castro AG, Pedrosa J. 2007. Mycolactone-Mediated Inhibition of Tumor Necrosis Factor Production by Macrophages Infected with *Mycobacterium ulcerans* Has Implications for the Control of Infection. Infect Immun 75:3979.

86. Bieri R, Bolz M, Ruf M-T, Pluschke G. 2016. Interferon-γ Is a Crucial Activator of Early Host Immune Defense against Mycobacterium ulcerans Infection in Mice. PLOS Negl Trop Dis 10:e0004450.

87. Phillips R, Horsfield C, Mangan J, Laing K, Etuaful S, Awuah P, Nyarko K, Osei-Sarpong F, Butcher P, Lucas S, Wansbrough-Jones M. 2006. Cytokine mRNA expression in *Mycobacterium ulcerans*-infected human skin and correlation with local inflammatory response. Infect Immun 74:2917-24.

88. Westenbrink BD, Stienstra Y, Huitema MG, Thompson WA, Klutse EO, Ampadu EO, Boezen HM, Limburg PC, van der Werf TS. 2005. Cytokine responses to stimulation of whole blood from patients with Buruli ulcer disease in Ghana. Clin Diagn Lab Immunol 12:125-9.

89. Torrado E, Fraga AG, Logarinho E, Martins TG, Carmona JA, Gama JB, Carvalho MA, Proenca F, Castro AG, Pedrosa J. 2010. IFN-gamma-dependent activation of macrophages during experimental infections by *Mycobacterium ulcerans* is impaired by the toxin mycolactone. J Immunol 184:947-55.

90. Flynn JL, Chan J. 2001. Immunology of tuberculosis. Annu Rev Immunol 19:93-129.
91. Magcwebeba T, Dorhoi A, du Plessis N. 2019. The Emerging Role of Myeloid-Derived Suppressor Cells in Tuberculosis. Front Immunol 10:917.
92. Boer MC, Joosten SA, Ottenhoff TH. 2015. Regulatory T-Cells at the Interface between Human Host and Pathogens in Infectious Diseases and Vaccination. Front Immunol 6:217.
93. Isailovic N, Daigo K, Mantovani A, Selmi C. 2015. Interleukin-17 and innate immunity in infections and chronic inflammation. J Autoimmun 60:1-11.
94. Greifenberg V, Ribechini E, Rossner S, Lutz MB. 2009. Myeloid-derived suppressor cell activation by combined LPS and IFN-gamma treatment impairs DC development. Eur J Immunol 39:2865-76.
95. Jiang M, Chen J, Zhang W, Zhang R, Ye Y, Liu P, Yu W, Wei F, Ren X, Yu J. 2017. Interleukin-6 Trans-Signaling Pathway Promotes Immunosuppressive Myeloid-Derived Suppressor Cells via Suppression of Suppressor of Cytokine Signaling 3 in Breast Cancer. Front Immunol 8:1840.
96. Miossec P, Kolls JK. 2012. Targeting IL-17 and TH17 cells in chronic inflammation. Nat Rev Drug Discov 11:763-76.
97. Forbes BR, Wannan JS, Kirkland WB. 1954. Indolent cutaneous ulceration due to infection with *Mycobacterium ulcerans*. Med J Aust 41:475-9.
98. Adusumilli S, Mve-Obiang A, Sparer T, Meyers W, Hayman J, Small PL. 2005. *Mycobacterium ulcerans* toxic macrolide, mycolactone modulates the host immune response and cellular location of M. ulcerans in vitro and in vivo. Cell Microbiol 7:1295-304.
99. Ogbechi J, Ruf MT, Hall BS, Bodman-Smith K, Vogel M, Wu HL, Stainer A, Esmon CT, Ahnstrom J, Pluschke G, Simmonds RE. 2015. Mycolactone-Dependent Depletion of Endothelial Cell Thrombomodulin Is Strongly Associated with Fibrin Deposition in Buruli Ulcer Lesions. PLoS Pathog 11:e1005011.
100. George KM, Pascopella L, Welty DM, Small PL. 2000. A *Mycobacterium ulcerans* toxin, mycolactone, causes apoptosis in guinea pig ulcers and tissue culture cells. Infect Immun 68:877-83.
101. Hong H, Gates PJ, Staunton J, Stinear T, Cole ST, Leadlay PF, Spencer JB. 2003. Identification using LC-MSn of co-metabolites in the biosynthesis of the polyketide toxin mycolactone by a clinical isolate of *Mycobacterium ulcerans*. Chem Commun (Camb):2822-3.
102. Laemmli UK. 1970. Cleavage of structural proteins during the assembly of the head of bacteriophage T4. Nature 227:680-5.
103. Sekiya T, Yamagishi J, Gray JHV, Whitney PG, Martinelli A, Zeng W, Wong CY, Sugimoto C, Jackson DC, Chua BY. 2017. PEGylation of a TLR2-agonist-based vaccine delivery system improves antigen trafficking and the magnitude of ensuing antibody and CD8(+) T cell responses. Biomaterials 137:61-72.
104. Wijayadikusumah AR, Zeng W, McQuilten HA, Wong CY, Jackson DC, Chua BY. 2019. Geometry of a TLR2-Agonist-Based Adjuvant Can Affect the Resulting Antigen-Specific Immune Response. Mol Pharm 16:2037-2047.
105. Chua BY, Pejoski D, Turner SJ, Zeng W, Jackson DC. 2011. Soluble proteins induce strong CD8+ T cell and antibody responses through electrostatic association with simple cationic or anionic lipopeptides that target TLR2. J Immunol 187:1692-701.
106. Beasley TM, Erickson S, Allison DB. 2009. Rank-based inverse normal transformations are increasingly used, but are they merited? Behav Genet 39:580-95.
107. Pedregosa F, Varoquaux G, Gramfort A, Michel V, Thirion B, Grisel O, Blondel M, Prettenhofer P, Weiss R, Dubourg V, Vanderplas J, Passos A, Cournapeau D, Brucher M, Perrot M, Duchesnay E. 2011. Scikit-learn: Machine Learning in Python. J Mach Learn Res 12:2825-2830.

957 108. Polsterl S, Gupta P, Wang L, Conjeti S, Katouzian A, Navab N. 2016. Heterogeneous
958 ensembles for predicting survival of metastatic, castrate-resistant prostate cancer patients.
959 F1000Res 5:2676.
960 109. Evers L, Messow CM. 2008. Sparse kernel methods for high-dimensional survival data.
961 Bioinformatics 24:1632-8.
962 110. Shivaswamy PK, Chu W, Jansche M. 2007. A support vector approach to censored targets.
963 Icdm 2007: Proceedings of the Seventh Ieee International Conference on Data Mining
964 doi:10.1109/Icdm.2007.93:655-+.
965 111. van der Maaten L, Hinton G. 2008. Visualizing Data using t-SNE. J Mach Learn Res 9:2579-
966 2605.
967 112. Team RC. 2014. R: A Language and Environment for Statistical Computing, R Foundation for
968 Statistical Computing, Vienna, Austria. http://www.R-project.org/.
969 113. Bolz M, Kerber S, Zimmer G, Pluschke G. 2015. Use of Recombinant Virus Replicon Particles
970 for Vaccination against Mycobacterium ulcerans Disease. PLoS Negl Trop Dis 9:e0004011.
971 114. Fenner F. 1957. Homologous and heterologous immunity in infections of mice with
972 *Mycobacterium ulcerans* and *Mycobacterium balnei*. Am Rev Tuberc 76:76-89.
973

974

975 **Table 1. Summary of putative *M. ulcerans* vaccines tested in murine model of BU infection.**

Vaccine type	Description of components	*M. ulcerans* challenge dose	Test for mycolactone production[a]	Challenge model	Efficacy compared to BCG	Ref
DNA-based	pCDNA3 vector encoding Hsp65	10^4 AFB (strain 1615 ATCC35840)	Not mentioned	Tail	Less protective	(52)
DNA-based	V1Jns.tPA vector encoding Ag85A	3 x 10^4 AFB (strain 5150) or 10^5 AFB (strain 04-855)	Not mentioned	Footpad	Less protective	(32, 33)
DNA-based	Primary vaccination with V1Jns.tPA plasmid encoding mycolactone polyketide domains and boosted with recombinant domain proteins emulsified in Gerbu adjuvant.	10^5 AFB (strain 1615)	Not mentioned	Footpad	Less protective	(49)
Viral	Vesicular stomatitis virus (VSV) replicon particles expressing *M. ulcerans* codon optimised antigens MUL_2232 and MUL_3720	30µl of 2.8 x 10^5 CFU/ml stock (8.4 x 10^3 CFU/dose) (strain S1013)	Not mentioned	Footpad	Less protective	(113)
Subunit	MUL2232 and MUL3720 adjuvanted with GLA-SE (EM408)	1.5 x 10^6 or 1.5 x 10^5 CFU (strain S1013)	Not mentioned	Footpad	Less protective	(34)
Live Cell	*M. ulcerans*	$10^{6.3}$ or $10^{4.3}$ viable bacteria	Not mentioned	Footpad	Less protective	(114)
Live cell	*M. marinum*	10^5 bacteria (strain 1615)	Not mentioned	Footpad	More protective[b]	(35)
Live cell recombinant	*M. marinum* expressing Ag85A (on vector)	10^5 bacteria (strain 1615)	Not mentioned	Footpad	More protective[b]	(35)
Live cell recombinant	*M. bovis* BCG expressing Ag85A (on vector pMV261)	10^5 bacteria (strain 1615)	Not mentioned	Footpad	More protective	(36)
Live cell recombinant	*M. bovis* BCG expressing Ag85B-EsxH fusion protein Ag85A (on vector pMV261)	10^5 bacteria (strain 1615)	Not mentioned	Footpad	More protective	(37)

Inactivated whole cell	Mycolactone-negative *M. ulcerans* (strain 5114)	4 $\log_{10}$ or 3 $\log_{10}$ CFU (strain 98-912)	Not mentioned	Footpad	Less protective	(25)
Inactivated whole cell	Mycolactone-deficient attenuated *M. ulcerans* (strain ATCC19423)	10^6 bacteria (strain TMC1615)	Not mentioned	Footpad	Not compared	(54)
Inactivated whole cell	Formalin-treated *M. ulcerans* (strain TMC1615)	10^6 bacteria (strain TMC1615)	Not mentioned	Footpad	Not compared	(54)
Inactivated whole cell	Dewaxed *M. ulcerans* (strain TMC1615)	10^6 bacteria (strain TMC1615)	Not mentioned	Footpad	Not compared	(54)
Phage	Mycobacteriophage D29 (therapeutic vaccine)	5.5 $\log_{10}$ AFB (strain 1615)	Not mentioned	Footpad	Not comparable	(53)

[a] Identifying whether the bacterial culture used for challenge was assessed for mycolactone production before infection.
[b] Vaccine was more protective than the BCG vaccine, however all mice eventually developed footpad swelling.

Table 2: High-scoring immune features associated with delayed bioluminescence

Feature number	Feature	Tissue site	Association with delayed bioluminescence	Concordance index
1.	IFN-γ	spleen	negative	0.786
2.	IL-2	spleen	positive	0.769
3.	IL-6	spleen	negative	0.759
4.	TNF-α	spleen	negative	0.745
5.	IL-2	lymph node	positive	0.715
6.	IFN-γ $CD4^+$ T-cell	spleen	negative	0.707

Figures:

Figure 1

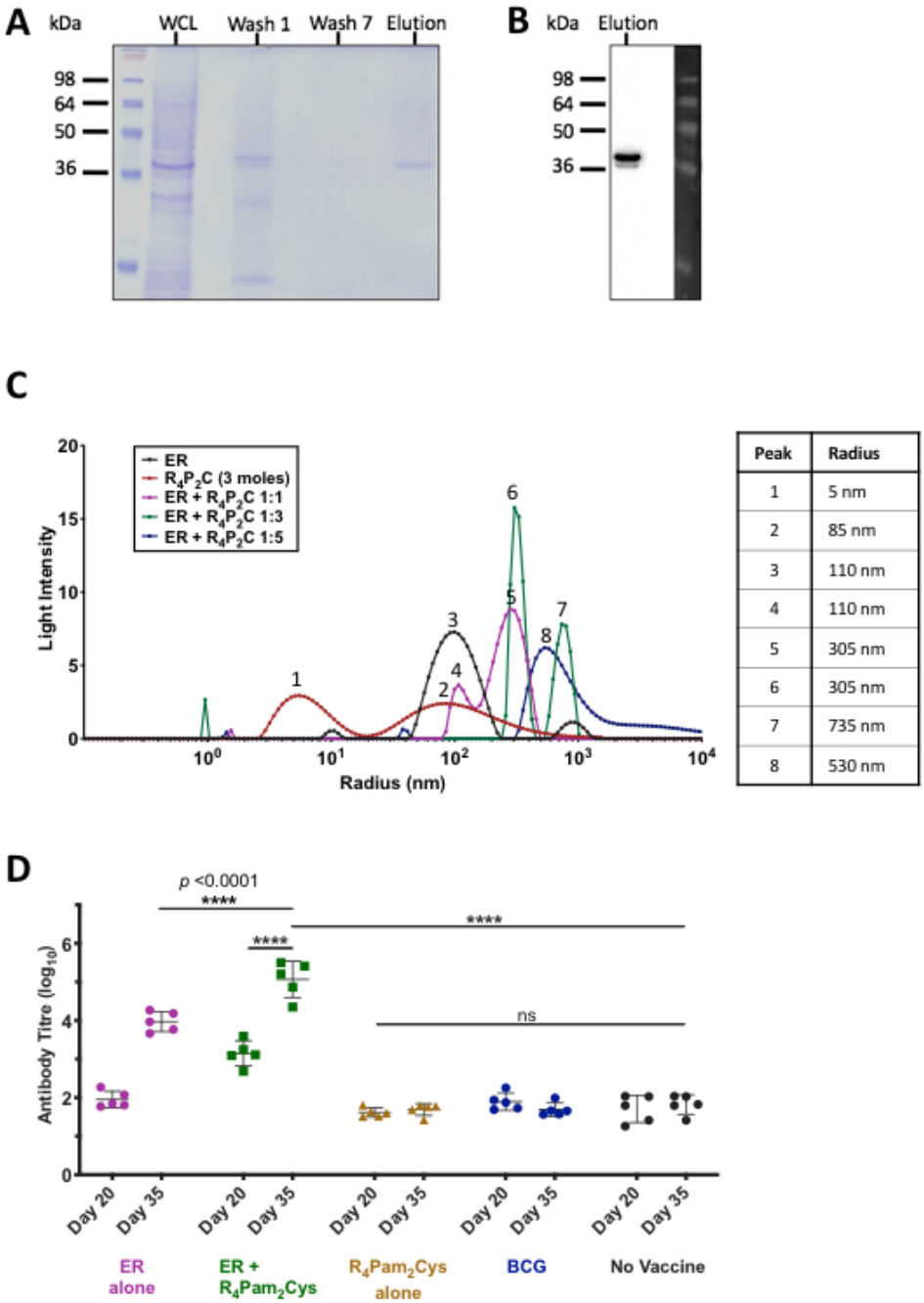

Figure 1. Analysis of purified recombinant ER protein antigen characteristics and formulation with R_4Pam_2Cys. (A) The presence of recombinant ER protein (~37 kDa) was monitored by SDS-PAGE at each stage of the purification process; Lane: 1 - Whole cell lysate (WCL), Lane 2 - Wash 1, Lane 3 - Wash 7 and Lane 4 – ER protein elution (containing 10 µg protein). **(B)** Western Blot using an anti-

990 6xHIS-tag antibody to detect the presence of a single band corresponding to the correct molecular
991 weight of the ER protein in the final eluate. **(C)** To analyse the formation of antigen-lipopeptide
992 complexes, a constant amount of antigen was mixed with lipopeptide at different
993 protein:lipopeptide molecular ratios in 50µl of PBS. The size distribution of particles was then
994 analysed by DLS with each profile depicting the hydrodynamic radius (nm) of complexes in each
995 solution. The average radius of each formulation is highlighted in the accompanying table. **(D)**
996 BALB/c mice (n=5/group) were vaccinated on day 0 and day 21 with R_4Pam_2Cys alone, ER antigen
997 alone or antigen formulated with R_4Pam_2Cys or vaccinated with BCG on day 0 only. Total serum
998 (IgG) antibody against recombinant ER protein were measured by ELISA after the primary dose (day
999 20) and two weeks after the secondary dose (day 35). Statistical tests were conducted at the 5%
1000 significance level. The null hypothesis was rejected if there was a significant difference in mean
1001 antibody responses between treatment groups. Note: *$p < 0.05$, **$p < 0.01$, ***$p < 0.001$ or ****p
1002 < 0.0001. The error bars represent standard deviation (n=5).
1003
1004
1005

1006 Figure. 2

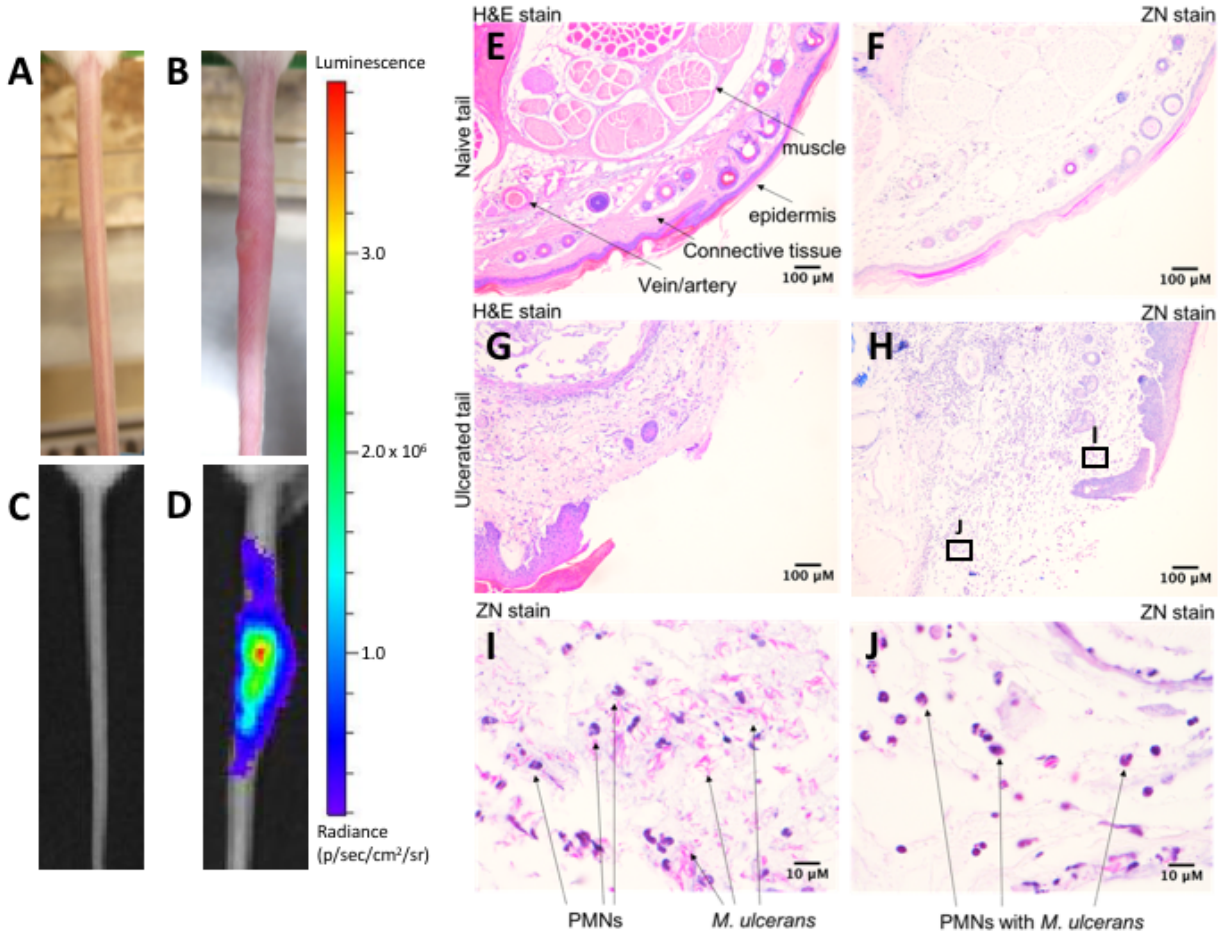

1007

1008 **Figure 2. Characterisation of infection using a low-dose bioluminescent *M. ulcerans* strain.**

1009 Representative light camera images of tails from **(A)** an uninfected BALB/c mouse or **(B)** at the point

1010 of ulceration (16 weeks) following intradermal inoculation with 20 CFU of bioluminescent *M.*

1011 *ulcerans*. **(C, D)** The same tails were visualised under an IVIS camera to detect and quantify

1012 bioluminescence intensity (as photons/sec). Histological cross section of an **(E, F)** uninfected or **(G,**

1013 **H)** infected tail tissue following haematoxylin & eosin (H&E) and Ziehl-Neelson (ZN) staining.

1014 Zoomed images of the regions indicated within the denoted boxes of **(H)** and depicts the presence

1015 of polymorphonuclear cells (PMNs) and acid-fast bacilli (ZN staining) within tissue **(I, J)**.

1016

1017 Figure. 3

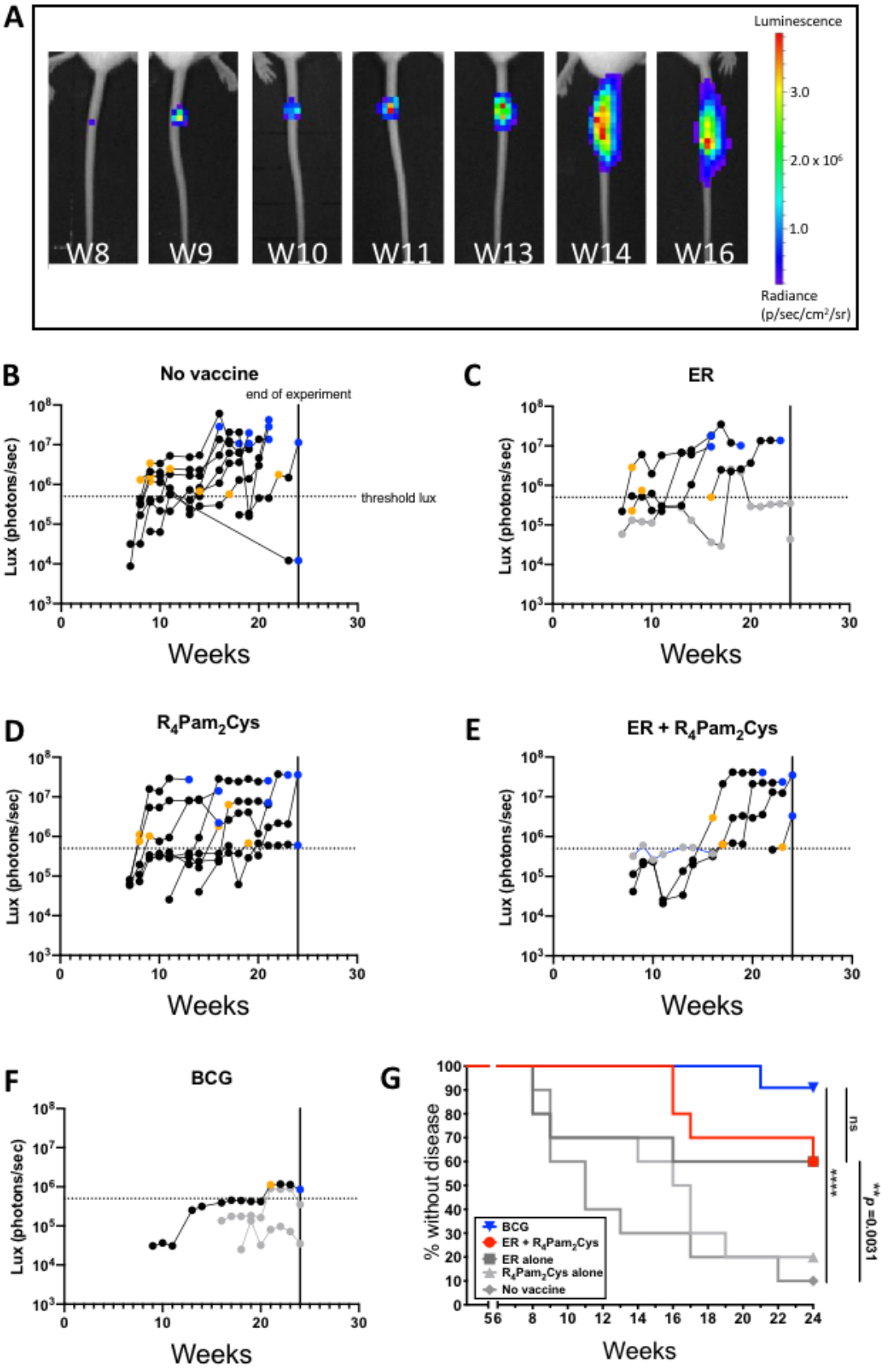

1018

1019 **Figure 3. Development of BU over time after vaccination**. (A) Tails of mice were intradermally

1020 infected with 20 CFU of bioluminescent *M. ulcerans* and imaged weekly by IVIS. Representative

1021 panels depict the weekly progression of bioluminescent *M. ulcerans* burden in the tail of an
1022 unvaccinated mouse over the course of 16 weeks expressed as photons/second. BALB/c mice
1023 (n=10/group) were left **(B)** unvaccinated, or vaccinated on day 0 and day 21 with **(C)** ER antigen
1024 alone, **(D)** R_4Pam_2Cys alone, , **(E)** ER antigen formulated with R_4Pam_2Cys or **(F)** on day 0 with BCG
1025 followed by challenge on week 5 with bioluminescent *M. ulcerans*. Threshold bioluminescence
1026 (threshold lux) for disease was defined as ≥5 x 10^5 photons/second (p/s) as mice that reached this
1027 level typically progressed to the clinical (ethical) end point. Mice were classified as diseased if they
1028 reached this end point within the 24-weeks following challenge or if their bioluminescence value at
1029 week 24 was ≥5 x 10^5 p/s. Mice were classified as protected if they did not reach this clinical end
1030 point and their bioluminescence value was <5 x 10^5 photons/second. The data point depicting when
1031 an infected mouse first exhibited bioluminescence at ≥5 x 10^5 p/s is represented with a yellow
1032 symbol. The data point denoting when a mouse reached clinical endpoint is represented with a blue
1033 symbol. Protected mice with detectable bioluminescence are depicted as grey symbols. **G.** Time to
1034 bioluminescence measured by IVIS. A survival curve was utilised to analyse the time (weeks) taken
1035 for each BU diseased mouse to first reach threshold bioluminescence ≥5 x 10^5 photons/second. BCG
1036 group (upside down triangle) is labelled in blue, ER + R_4Pam_2Cys (circle) is red, and ER alone (square),
1037 R_4Pam_2Cys alone (upright triangle) and no vaccine (diamond) groups are depicted in grey. Statistical
1038 tests were conducted at the 5% significance level. The null hypothesis was rejected if there was a
1039 significant difference in survival between groups. Note: *$p < 0.05$, **$p < 0.01$, ***$p < 0.001$ or ****p
1040 < 0.0001.
1041

1042 Figure 4

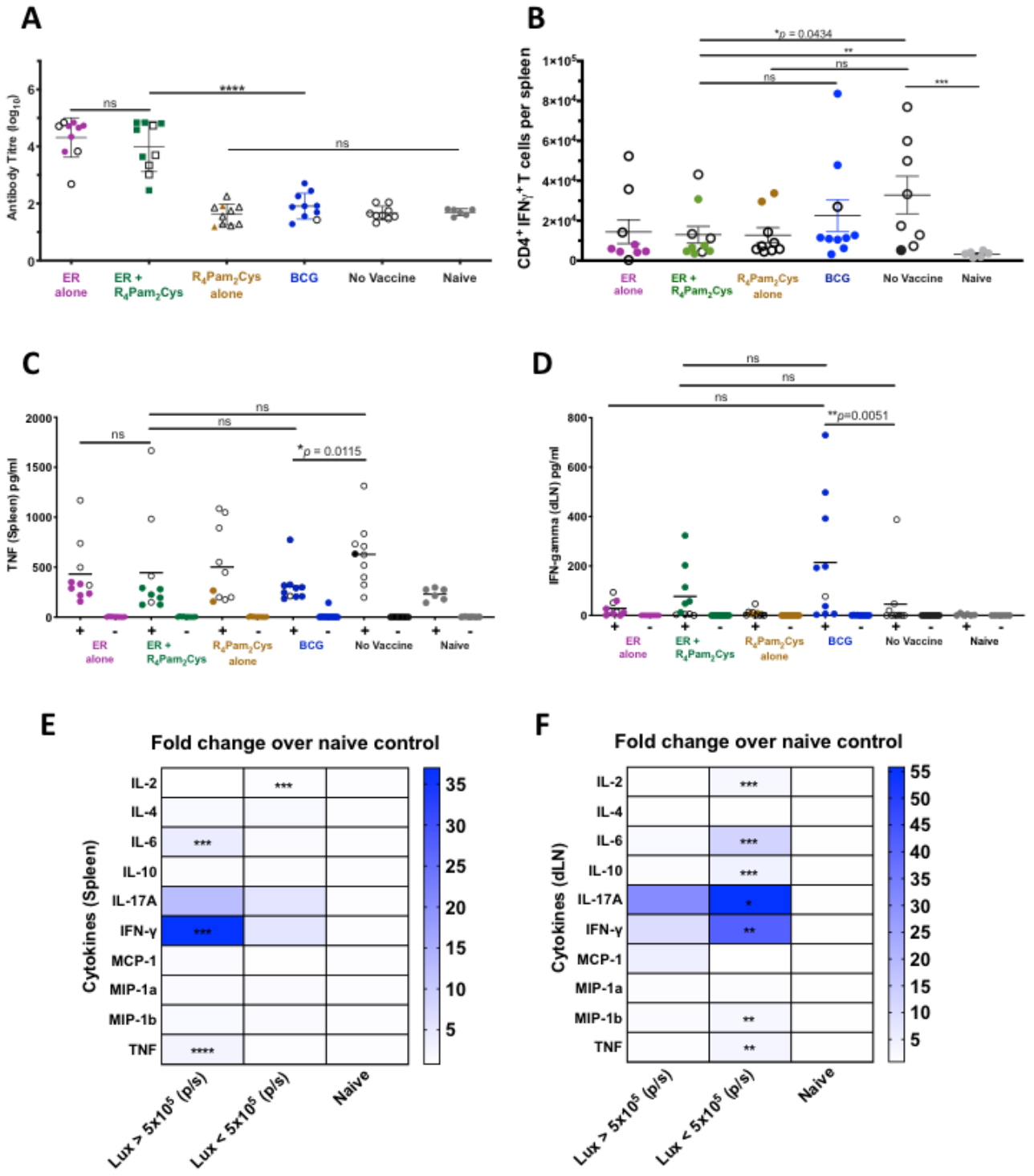

1043

1044 **Figure 4. Immune responses after *M. ulcerans* infection.** BALB/c mice (n=10/group) were left

1045 unvaccinated or vaccinated on day 0 and day 21 with ER antigen alone, ER antigen formulated with

1046 R_4Pam_2Cys, R_4Pam_2Cys alone, or on day 0 with BCG followed by challenge on day 36 with

1047 bioluminescent *M. ulcerans*. **(A)** Total serum (IgG) antibody against recombinant ER protein were

1048 measured by ELISA after the experimental end point. All data points for diseased mice

(bioluminescence ≥5 x 10^5 p/s) are depicted with white symbols. Statistical tests were conducted at the 5% significance level. The null hypothesis was rejected if there was a significant difference in mean antibody responses between treatment groups. The error bars represent standard deviation. **(B)** After experimental end point was reached, CD4+ IFN-γ+ T cells were enumerated from the spleen of mice in response to ER protein. The null hypothesis was rejected if there was a significant difference in mean CD4+ IFN-γ+ T cells between treatment groups. Once experimental end point was reached, cytokines from draining lymph nodes and spleens of *M. ulcerans* challenged mice were also measured in response to *in vitro* cell stimulation with recombinant ER protein (Supplementary Table S1). Shown here are cytokine titres **(C)** IFN-γ produced from immune cells in the draining lymph nodes and **(D)** TNF produced from immune cells in the spleen. The null hypothesis was rejected if there was no difference in mean cytokine titres between treatment groups. The black bars represent the mean. Fold change of mean cytokine titres from protected mice (bioluminescence <5 x 10^5 p/s) and diseased mice (bioluminescence ≥5 x 10^5 p/s) over naïve mice were compared in the (**E)** spleen and (**F)** draining lymph nodes. The null hypothesis was rejected if there was a significant difference in mean cytokine titres between treatment groups. All statistical tests were conducted at the 5% significance level. Note: *$p < 0.05$, **$p < 0.01$, ***$p < 0.001$ or ****$p < 0.0001$.

Figure 5

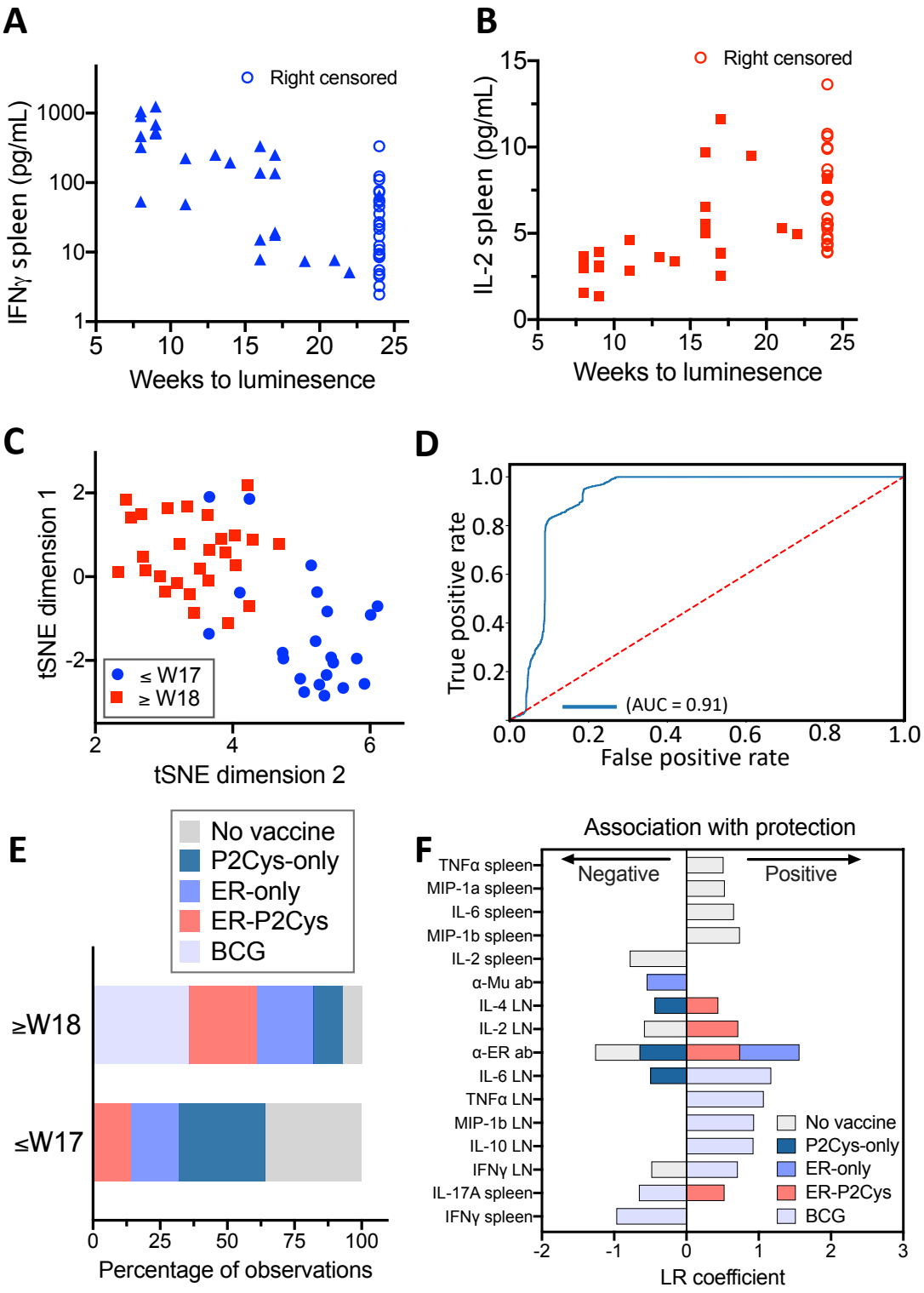

Figure 5. Statistical modelling to identify immune parameters (features) associated with vaccine protection. Univariate Cox Proportional hazards models were specified for each of the 28 immunological features to test their association with the response variable (time-to-bioluminescence measured in weeks). The resulting concordance index (CI) scores were obtained

and the six features with a CI >0.7 were retained. The inverse associations of the top two features **(A)** IFN-γ and **(B)** IL-2 produced in murine splenocytes at the experimental end-point. **(C)** Plot depicting a two-dimensional representation of the top six features that associate with time-to-bioluminescence from the unsupervised t-SNE. The shapes/colours indicate the two groups identified through K-means clustering, of bioluminescence by 8-17 weeks or at 18 weeks and beyond (up to 24 weeks). **(D)** Receiver operator curve (and corresponding area under curve), displaying the trade-off between sensitivity and specificity across all thresholds for 1,000 random train-test splits of a logistic regression classifier (90% of observations used for training). The red dotted line depicts the expectation of a random classifier and the blue line depicts the model performance. **(E)** Proportion of observations across treatment groups for each of the classes both 8-17 weeks and 18-24 weeks and those with no detection. **(F)** Group-specific univariate logistic regression analyses for each of the five treatment groups. Model coefficients were used to determine both the strength and direction of association of each feature with that of each treatment group. Depicted are those features with a corresponding p-value<0.05 (Table S2).

1090 **Supplementary data**

1091 **Table S1** - Vaccination data

1092 **Table S2** - Summary of group-specific univariate logistic regression coefficients

1093